RAD52 prevents accumulation of Polα-dependent replication gaps at perturbed replication forks in human cells

[1,2] Ludovica Di Biagi, [1] Eva Malacaria, [1,2] Francesca Antonella Aiello, [1] Pasquale Valenzisi, [1] Giorgia Marozzi, [1] Annapaola Franchitto and Pietro Pichierri [1,2 §]

1 Mechanisms, Biomarkers and Models Section, Department of Environment and Health, Istituto Superiore di Sanità - Viale Regina Elena 299, 00161 Rome (Italy)
2 Istituto Nazionale Biostrutture e Biosistemi - Roma Area Research Unit - Via delle Medaglie d'Oro 305, 00136 Rome (Italy)

§ Author to whom correspondence should be addressed:

Pietro Pichierri
Tel. +39 0649902355
Fax +39 0660513138
pietro.pichierri@iss.it

Running title: RAD52 and replication gaps

ABSTRACT

Replication gaps can arise as a consequence of perturbed DNA replication and their accumulation might undermine the stability of the genome. Loss of RAD52, a protein involved in the regulation of fork reversal, promotes accumulation of parental ssDNA gaps during replication perturbation. Here, we demonstrate that this is due to the engagement of Polα downstream of the extensive degradation of perturbed replication forks after their reversal, and is not dependent on PrimPol. Polα is hyper-recruited at parental ssDNA in the absence of RAD52, and this recruitment is dependent on fork reversal enzymes and RAD51. Of note, we report that the interaction between Polα and RAD51 is stimulated by RAD52 inhibition, and Polα-dependent gap accumulation requires nucleation of RAD51 suggesting that it occurs downstream strand invasion. Altogether, our data indicate that RAD51-Polα-dependent repriming is essential to promote fork restart and limit DNA damage accumulation when RAD52 function is disabled.

INTRODUCTION

The response to perturbed replication fork progression is crucial to prevent accumulation of unreplicated DNA regions, DNA damage and genomic rearrangements [1–4]. For this reason, cells evolved multiple mechanisms of protection that deal with impaired replication fork progression and replication stress [3,5,6]. A crucial step in this process is represented by the DNA remodelling occurring at perturbed or stalled replication forks. Fork remodelling involves the reannealing of the two nascent strands promoted by regression of the replication fork structures producing a four-way DNA intermediate called reversed fork (RF) [7]. This reaction has been first discovered in bacteria where it is catalysed by RecG while, in human cells, involves multiple factors including SMARCAL1, ZRANB3 and the homologous recombination protein RAD51 [6,8,9]. If on one hand the RF contributes to protect nascent ssDNA, on the other hand it produces a DNA end that can be attacked by nucleases. Thus, the RF extruded strand is protected by unscheduled and extensive degradation by BRCA2, RAD51 and other proteins acting as "barriers" against the action of MRE11 and EXO1 [5,10–12]. Pathological DNA transactions at replication forks is also counteracted by proteins that regulate fork remodelling, such as ATR or RADX [13,14]. In addition, we have recently uncovered a role for RAD52 in preventing fork degradation by regulating the extent of SMARCAL1 having access to the DNA replication fork [15]. Since the reversed fork can be also a target for exo- or endonucleases [3,5], cells balance its usage with other mechanism granting continuation of DNA synthesis. Recently, it has been reported that replication fork reversal and repriming act as parallel "fork recovery" pathways: too limited fork reversal upregulates repriming and vice versa [16–18]. In yeast, repriming under perturbed replication involves the Polα primase but recent reports indicated that a specialised Primase-Polymerase, PrimPol, takes over in humans [19–22]. Repriming at perturbed replication forks leads to accumulation of ssDNA gaps that needs to be subsequently repaired to prevent accumulation of unreplicated DNA in mitosis [23,24]. Intriguingly, abrogation of RAD52 function stimulates formation of parental ssDNA although it does not overtly affect ability of fork to restart after stalling [15].

Here, we used multiple cell biology techniques and cell models to investigate if loss of RAD52 function could affect the repriming in response to perturbed replication. We show that loss of RAD52 function stimulates the accumulation of parental ssDNA gaps and that those gaps are not dependent on PrimPol but rather are dependent on Polα. In the absence of a functional RAD52, origin-independent Polα recruitment at DNA is stimulated. Such origin-independent Polα recruitment occurs downstream fork reversal and degradation, and is mechanistically-linked to inability to induce MUS81-dependent DSBs at the degraded reversed forks. Intriguingly, the

recruitment of Polα licensed by RAD52 inactivity requires RAD51 nucleofilaments and involves binding with RAD51 itself. Under these conditions, engagement of this Polα-mediated repriming is instrumental in ensuring maximal fork recovery and DNA damage avoidance.

Therefore, our results uncover a novel mechanism of repriming granting fork recovery and protecting from genome instability engaged when aberrant or partial DNA transactions occur at perturbed replication forks.

RESULTS

RAD52 prevents formation of gaps at perturbed replication forks

Perturbed replication forks are extensively degraded in the absence of RAD52, however, a large part of them retains ability to resume DNA synthesis [15]. Two main pathways are used to resume degraded DNA replication forks: recombination or repriming [3,24,25]. Since RAD52 inactivation should prevent DSB formation at degraded forks and subsequent break-induced replication [11], we analysed the presence of template gaps, which possibly derives from repriming events, upon replication arrest. To this end, we monitored the exposure of ssDNA on the parental strand in cells treated with the RAD52 inhibitor ECG (RAD52i; [26]) and 2mM HU after labelling DNA for 24h with Iododeoxyuridine (IdU) (Figure 1A). Parental ssDNA was analysed at multiple recovery times by a native IdU detection [27] (Figure 1A). We found that parental ssDNA can be detected in RAD52-proficient and deficient cells after 2h of recovery, however, parental ssDNA was significantly higher in cells inhibited of RAD52 after 4h of recovery and persisted also at 18h of recovery.

Consistent with results obtained with the RAD52i, stable depletion of RAD52 using RNAi [15] also led to high and persistent levels of parental ssDNA during recovery from replication arrest (Figure 1B). To exclude that parental ssDNA might derive from extensive MRE11-mediated fork degradation and to validate our data in a different background, we evaluated the presence of ssDNA during recovery in U2OS cells treated with the RAD52i alone or in combination with the MRE11 inhibitor MIRIN. As shown in Figure 1C, inhibition of MRE11 during replication arrest did not have much effect on parental ssDNA levels in RAD52-deficient cells. To corroborate our data, we decided to analyse the presence of parental ssDNA also in U2OS cells treated with a low dose of HU (0.5mM), which is widely used to evaluate ssDNA gaps as it slows down replication without inducing stalling [28]. Some exposure of parental ssDNA was detected in wild-type cells treated with 0.5mM HU, however, inhibition of RAD52 (Figure 1D) or its stable depletion (Figure S1) greatly increased the amount of parental ssDNA detected by IF, especially at 4h of treatment. Upon treatment with 0.5mM HU, the level of parental ssDNA was not affect by MIRIN in RAD52i-treated cells while, unexpectedly, it was increased in wild-type U2OS cells (Figure 1D).

To demonstrate that the elevated levels of parental ssDNA detected in the absence of RAD52 correlated with the presence of replicative gaps, we performed the S1 DNA fiber assay [29]. We pulse-labelled cells with CldU followed by labelling with IdU and treatment with 0.5mM HU, in the presence or not of the RAD52i (see scheme in Figure 1E). After treatments, cells were exposed to the S1 nuclease to cut at regions of ssDNA before obtaining DNA fibers. Thus, gap-containing replication tracts were expected to be shorter after treatment with S1 nuclease leading to a

IdU/CldU ratio < 1. Following treatment with 0.5mM HU, cells inhibited of RAD52 showed a IdU/CldU ratio that is comparable to that of non-inhibited cells (Figure 1E). Treatment with S1 nuclease significantly reduced the IdU/CldU ratio in cells inhibited of RAD52 but not in wild-type cells (Figure 1E), confirming that RAD52 deficiency induces the accumulation of parental DNA gaps at perturbed replication fork.

Altogether, these results show that inhibition of RAD52 or its depletion leads to the formation of parental gaps upon replication perturbation.

Inhibition of RAD52 stimulates Polα-dependent gaps

We observed that loss or inhibition of RAD52 induces the accumulation of parental gaps at perturbed replication forks and that those gaps are not the consequence of MRE11-dependent degradation. A similar phenotype has been reported in BRCA-deficient cells and is dependent on a defect in regulating correct metabolism of Okazaki fragments and to PrimPol-mediated repriming [16,30,31]. To test if template gaps might derive from the repriming activity of PrimPol at perturbed replication forks, we inhibited RAD52 in wild-type or PrimPol KO MRC5SV40 cells (MRC5 -/- PrimPol; [32]), and performed the DNA fiber S1 assay following 0.5mM HU. RAD52 mock-inhibited cells (WT) did not experience a significant accumulation of DNA gaps since the IdU/CldU ratios were not statistically different compared with the same cells treated with the S1 nuclease (Figure 2A). Consistently, PrimPol KO did not induce any rescue in the IdU/CldU ratios (Figure 2A). Inhibition of RAD52, as expected, resulted in accumulation of DNA gaps following replication perturbation as shown by the ability of S1 to shorten the IdU tract and determine IdU/CldU ratios < 1 (Figure 2A). Interestingly, S1 nuclease treatment reduced the IdU/CldU ratio in cells inhibited of RAD52 following replication perturbation even in the absence of PrimPol (Figure 2A), indicating that gaps are PrimPol-independent. We reasoned that, if PrimPol was not been involved in repriming, it should not recruit to the replication fork when RAD52 was inhibited. Thus, we decided to investigate the recruitment of PrimPol at parental ssDNA following fork arrest by *in situ* PLA [15,27] (Figure 2B). As none of the available anti-PrimPol antibodies is suitable for PLA, we added back GFP-PrimPol in PrimPol KO MRC5SV40 cells (Figure 2B). A low level of PrimPol was found associated with the parental ssDNA in untreated cells, irrespective of the function of RAD52 (Figure 2B). Surprisingly, although no DNA gaps were detected in mock-inhibited cells, treatment with HU significantly increased the association of PrimPol with parental ssDNA in these cells, however, recruitment of GFP-PrimPol at parental DNA was not stimulated by HU when RAD52 was inhibited (Figure 2B). To substantiate our PLA data, we performed chromatin fractionation in PrimPol KO MRC5SV40 cells transiently transfected with GFP-PrimPol and challenged with HU

2mM to induce replication fork arrest. Consistent with PLA data, cells accumulated PrimPol in chromatin in the absence of the RAD52 inhibitor while the normalised amount of GFP-PrimPol is not comparably increased in the presence of the inhibitor following HU, especially at 2h (Figure 2C). By contrast and consistent with recent data [17], depletion of SMARCAL1 led to an increase of PrimPol-dependent replicative gaps respect to the control-depleted cells (Figure S2A,B).

Having shown that replicative gaps accumulating following loss of RAD52 function are not PrimPol-dependent, we examined whether they might derive from Polα-dependent repriming. Indeed, in yeast, replication stress-associated gaps are produced by Polα when fork remodelling is hampered [20]. First of all, we investigated the recruitment of Polα at parental ssDNA by *in situ* PLA when RAD52 was inhibited (Figure 2D). *In situ* IdU-Polα PLA evidenced that recruitment of Polα to parental ssDNA was stimulated by inhibition of RAD52 already under unperturbed replication and, even more, after treatment with HU, although replication fork arrest increased the presence of Polα at parental ssDNA also in wild-type cells (Figure 2D and S3). Interestingly, inhibition of new origin firing by XL413, a CDC7 inhibitor (CDC7i), barely affected the low level of Polα association with ssDNA in mock-inhibited cells and, most importantly, did not reduce the increased association of POLA1 with ssDNA when RAD52 is inhibited (Figure S4A). Consistent with PLA, chromatin fractionation did not show any CDC7i-dependent reduction of chromatin-bound POLA1 in RAD52i-treated cells after replication arrest (Figure S4A), confirming that excess of Polα is recruited independently of firing at new or ancillary origins.

During unchallenged replication and in response to DNA damage, Polα is recruited at the replisome by Ctf-4/AND-1 [20,33]. Thus, we analysed if replication arrest-dependent recruitment of Polα at parental ssDNA in the absence of RAD52 was similarly dependent on the presence of AND-1. To this end, we depleted AND-1 in RAD52i-treated cells and assessed the interaction between Polα and DNA by PLA in response to replication perturbation (Figure S4C and D). As repeatedly observed in other experiments, inhibition of RAD52 greatly increased the amount of Polα detected at ssDNA after replication perturbation. Depletion of AND-1 slightly reduced the number of ssDNA-Polα spots in RAD52-proficent cells but reset the number of PLA spot to the level of non-inhibited cells when combined with RAD52i (Figure S4D).

Since inhibition of RAD52 stimulated the recruitment of Polα over that of PrimPol, we next analysed if inhibition of Polα might revert the excess of parental ssDNA in RAD52i-treated cells.

Treatment with a Polα inhibitor (ST1926; POLA1i) dramatically increases ssDNA at fork and eventually blocks replication [34]. Thus, we decided to titrate the amount of inhibitor selecting a concentration that does not impact significantly on DNA synthesis. We found that 0.3μM of POLA1i minimally reduced EdU incorporation in terms of number of positive cells and EdU

intensity (Figure S5) and thus we used this concentration to evaluate the exposure of ssDNA at 0.5mM HU (Figure 2E). As controls, we treated wild-type cells with 3μM of POLA1i, which was expected to accumulate ssDNA, and the CDC7i to only pinpoint the origin-independent function of Polα.

As expected, the high dose of POLA1i stimulated exposure of a huge amount of ssDNA in unperturbed cells (Figure 2E). The inhibition of RAD52 also stimulated formation of parental ssDNA, which was greatly decreased by the low-dose of POLAi and was no further influenced by CDC7i (Figure 2E). Interestingly, exposure of parental ssDNA in RAD52 mock-inhibited cells the low-dose of POLA1i did not affect also if combined with CDC7i.

To further assess the role of Polα in the formation of replicative gaps when RAD52 is inhibited, we performed the S1 DNA fiber assay in wild-type or PrimPol KO MRC5SV40 cells, treated or not with the low-dose of POLA1i. Our expectation was to find PrimPol-dependent gaps in RAD52-proficient cells and POLAi-sensitive gaps in cells inhibited of RAD52. Compared with cells treated with only HU, the inhibition of POLA1 did not reduce the IdU/CldU ratio in S1-treated fibers in wild-type cells (Figure 2F). In PrimPol KO cells, inhibition of POLA1 reduced the IdU/CldU ratio, possibly indicating that more gaps were introduced but independently on the PrimPol function (Figure 2F). Compared with mock-inhibited wild-type cells, inhibition of RAD52 reduced the IdU/CldU ratio of the S1-treated DNA fibers and the tract length ratio was not recovered in PrimPol KO cells (Figure 2F). In contrast, the low-dose of POLA1i increased significantly the IdU/CldU ratio in S1 DNA fibers from RAD52i-treated wild-type cells and, in a similar extent, also in the PrimPol KO (Figure 2F).

Collectively, these results indicate that inhibition of RAD52 stimulates an origin-independent recruitment of Polα that is linked to accumulation of replicative gaps through a Polα-dependent and PrimPol-independent mechanism.

Recruitment of Polα at perturbed replication forks depends on fork reversal

Since loss or inhibition of RAD52 stimulates degradation of reversed forks [15], we next investigated if stimulation of Polα recruitment could occur downstream fork reversal. Thus, we analysed association of Polα with parental ssDNA by PLA in MRC5SV40 cells stably expressing a doxycycline-regulated shSMARCAL1 cassette (Figure 3A; [35]). As expected, inhibition of RAD52 increased the presence of Polα at parental ssDNA and downregulation of SMARCAL1 reduced the PLA spots in RAD52-inhibited cells but barely in the control (Figure 3B). Similarly, depletion of SMARCAL1 reduced the amount of POLA1 detected in chromatin fractions from cells treated with the RAD52i (Figure 3C). To further confirm that the increased chromatin recruitment of POLA1

after inhibition of RAD52 would depend on the fork reversal, we decided to deplete ZRANB3, another key fork reversal enzyme, and performed chromatin fractionation experiments in HU-treated cells. Depletion of ZRANB3 by transient transfection with siRNAs (Figure 3D - input), reduced the amount of chromatin-associated POLA1 in RAD52i-treated cells, resetting the value to that observed in RAD52-proficient cells (Figure 3D - chromatin fraction).

The inhibition of RAD52 leads to fork degradation as unleashes recruitment of fork reversal enzymes [15]. A similar condition can be obtained by overexpressing SMARCAL1 [13]. Interestingly, when we induced a strong SMARCAL1 overexpression through the piggybac system in U2OS cells (Figure S6A) we failed to detect any increase of Polα-parental ssDNA PLA spots over the non-overexpressing cells and, unexpectedly, the number of PLA signals decreased upon SMARCAL1 overexpression (Figure S6B). This result was not the consequence of DSBs, which are stimulated by uncontrolled fork reversal [13] since it was not affected by depletion of MUS81, the nuclease contributing to DSBs formation in this conditions [13] (Figure S6A,B). Thus, engagement of Polα at perturbed forks when RAD52 is inhibited is not just a consequence of unrestrained fork reversal.

Since downregulation of fork reversal enzymes reduces the enhanced recruitment of Polα observed after inhibition of RAD52, we asked if it occurred downstream fork degradation stimulated by the absence of RAD52 [15]. Thus, we blocked fork degradation by exposing cells to the MRE11 inhibitor Mirin, alone or in combination with the RAD52i, and then analysed the presence of POLA1 at parental ssDNA following HU by PLA (Figure 3E). Mirin significantly, but not completely, decreased the recruitment of POLA1 at ssDNA in cells inhibited of RAD52 while it induced a small increase in wild-type cells (Figure 3E). These results indicate that recruitment of Polα stimulated by inhibition of RAD52 occurs, mainly, downstream fork remodelling and MRE11-dependent degradation [15]. Thus, we next investigated if this event might be a general response to fork reversal and degradation. To this aim, we performed PLA to assess the presence of POLA1 at parental ssDNA in BRCA2-depleted cells, the prototypical model of fork deprotection and MRE11-dependent degradation. Association of POLA1 with parental ssDNA in response to replication fork arrest was not increased by BRCA2 depletion as compared to mock-depleted cells and, most importantly, was not affected at all by preventing fork degradation with Mirin (Figure 4A, B). In contrast, recruitment at parental ssDNA of transiently-expressed GFP-tagged PrimPol was significantly stimulated by BRCA2 downregulation as compared to either wild-type or RAD52 inhibited cells (Figure 4C, D). Interestingly, and consistent with recent data [17], PrimPol engagement in the absence of BRCA2 was barely affected by MRE11 inhibition (Figure 4D).

In the absence of BRCA2, degraded reversed forks are subsequently converted into DSBs by MUS81/EME2 [36]. In contrast to depletion of BRCA2, loss or inhibition of RAD52 leads to fork

degradation but might concomitantly prevent MUS81 from inducing DSBs [15,37]. Thus, we wondered if blocking MUS81 in BRCA2-deficient, fork degradation-prone, cells might recapitulate what observed in the absence of active RAD52. To test this, we analysed the association or POLA1 with parental ssDNA by PLA in doxycycline-inducible shBRCA2 cells made knock-out for MUS81 by CRISPR-Cas9 [38] (Figure S7). As expected, in MUS81 wild-type cells, downregulation of BRCA2 did not affect the number of POLA1-ssDNA PLA spots (Figure 4E). As shown in Figure 4E, MUS81 knock-out did not stimulate POLA1-ssDNA association after replication fork arrest in BRCA2-proficient cells (i.e. in the absence of doxycycline; Doxy). However, an increased formation of POLA1-ssDNA PLA spots was clearly detected upon downregulation of BRCA2 in MUS81 knockdown cells (Figure 4E).

Altogether, these results indicate that, in response to replication fork arrest, POLA1 is *de novo* recruited downstream fork reversal following fork degradation and that its recruitment is dependent on impaired MUS81-dependent targeting of degraded forks.

The function of Polα at perturbed replication forks involves interaction with RAD51

We observe that recruitment of Polα in response to perturbed replication is origin-independent and depends on fork remodelling. In Xenopus extracts, Polα associates with Rad51 after replication arrest [39]. Thus, we tested if origin-independent recruitment of Polα that occurs following inhibition of RAD52 might involve association with RAD51. To this end, we first assessed the interaction between Polα and RAD51 by PLA after treatment with HU at different concentrations and times. Replication fork arrest resulted in the association of Polα with RAD51 already in cells in which RAD52 was not inhibited (U2OS WT), and this association increased with time becoming more evident at 4h of HU (Figure 5A). Interaction between Polα and RAD51 was higher and statistically significant in cells treated with the RAD52i, at both 2 and 4h of HU (Figure 5A). Similar to replication fork arrest, also replication fork perturbation by a low dose of HU resulted in enhanced interaction between Polα and RAD51 upon inhibition of RAD52 (Figure 5B). To further confirm that RAD52 inhibition stimulated Polα recruitment and association with RAD51 at perturbed replication forks we performed correlative single-molecule localisation microscopy by dSTORM. Active replication forks were labelled with a short EdU pulse before challenging replication with 0.5mM HU in the presence or not of RAD52i (Figure 5C). After filtering out single labelling sites, co-localisation at the nanometry-scale was then assessed in tri-colour dSTORM through the analysis of the variation of signal clustering involving EdU-Polα or Polα-RAD51 at EdU+ sites (Figure 5D). These analyses confirmed the increase in the fraction of Polα at EdU+ sites observed with PLA and revealed that RAD52 inhibition resulted in a shift of the fraction of RAD51 molecules that engage

in single interaction with the fork to the benefit of the fraction involved in the association with Polα at the EdU+ sites (Figure 5D, E). Furthermore, topology inspection suggested that Polα is found almost always at the end of the EdU signal that is preceded by or embedded into the RAD51 signal in the clustered analysis.

We next investigated if RAD51 might be functionally required in the hyper-recruitment of Pola observed after inhibition of RAD52. Thus, we evaluated the association of Polα with parental ssDNA after treatment with 2mM or 0.5mM HU in the presence or not of the RAD52i by PLA when functionality of RAD51 was inhibited using the B02 compound (RAD51i). As shown in Figure 6A, in RAD52-proficient cells (WT), inhibition of RAD51 increased rather than decreased the level of association between Polα and ssDNA upon replication arrest. In contrast, inhibition of RAD51 led to a striking reduction in the number of PLA spots when RAD52 was inhibited, indicating a reduction in association of Polα with ssDNA following replication arrest (Figure 6A). Of note, inhibition of RAD51 set back the level of Polα-ssDNA interaction to that detected in wild-type cells. To confirm this striking RAD51 dependency observed in the HU-induced recruitment of Polα when RAD52 is inhibited, we performed Western blotting in chromatin fractions from cells treated with 2mM HU for 4h. Recapitulating what observed by PLA, analysis of chromatin-associated proteins showed more POLA1 associated with DNA in cells treated with RAD52i and HU, and confirmed that concomitant inhibition of RAD51 reduced this association (Figure 6B). In RAD52 inhibited cells, the association of Polα with parental ssDNA and the exposure of parental ssDNA, a readout of gap accumulation (see Figure 2), was RAD51-dependent also following treatment with 0.5mM HU (Figure S8).

RAD51 is required prior to fork reversal to promote remodelling and later to protect the extruded strand [40,41]. In addition, RAD51 might be required to promote recombination from the ssDNA produced at the reversed fork. To discriminate between the different roles of RAD51, we decided to deplete RAD51 using different concentrations of the J11 siRNA. Indeed, high concentrations have been reported to interfere with the function before fork reversal, which requires less RAD51 molecules, while low concentrations are sufficient to interfere with the function after fork reversal (fork protection or strand-invasion), which requires more RAD51 molecules [14].

As shown in Figure 6C, transfection with 2pmol of J11 siRNA led to only minor changes in the amount of RAD51 while 20pmol of oligos reduced the protein level of more than 80% respect to the mock-transfected control. In RAD52 mock-inhibited cells (WT), recruitment of Polα at parental ssDNA in response to replication fork arrest was not affected by transfection with either 2pmol or 20pmol of the J11 RAD51 siRNA (Figure 6D). However, when RAD52 was inhibited, transfection with 2pmol of RAD51 J11 siRNA was nonetheless sufficient for a significant reduction in the level

of Polα-ssDNA binding (Figure 6D). Following RAD52 inhibition, the HU-stimulated association between Polα and the ssDNA was also reduced by 20pmol of RAD51 J11 siRNA (Figure 6D), and this is consistent with the observed dependency of this Polα recruitment from fork reversal (see Figure 3). To further substantiate our observations, we analysed if inhibition of RAD51 before or in the last 2h of the HU treatment differently affected the association of Polα and ssDNA (scheme in Figure 6E). In the absence of RAD52i, inhibition of RAD51, either before or during the last 2h of HU treatment, did not affect the recruitment of Polα as seen by PLA (Figure 6E). In sharp contrast, inhibition of RAD51 decreased the enhanced Polα-ssDNA association observed when RAD52 was inhibited, and even exposure of cells to the RAD51i in the last 2h of treatment was effective (Figure 6E).

These results indicate that the origin-independent Polα recruitment and parental ssDNA accumulation stimulated by loss of RAD52 function during replication perturbation are dependent on the function of RAD51 upstream and downstream the reversed fork.

Polα recruitment occurs downstream extended degradation in lagging strand at perturbed replication forks

Our results suggest that stable RAD51 nucleofilaments are required for Polα recruitment downstream fork reversal when replication is perturbed in the absence of RAD52. This event might implicate nucleolytic reset of the reversed fork before repriming by Polα. Under these conditions, we reasoned that proximity of Polα with nascent DNA would have been detectable well behind the fork. To test this hypothesis, we pulse-labelled active replication forks with EdU followed by chase in EdU-free medium and treatment with 0.5mM HU, to slow-down replication, in the presence or not of MIRIN and RAD52i (Figure 7A). Assuming 1/10th of normal replication fork rate in 0.5mM HU (~ 0.1 vs. 1Kb/min; [42]), these pulse and chase experiments were expected to locate labelled nascent DNA at different positions respect to the delayed fork: close to it or far to it (Figure 7A). At the 5min chase time-point, SIRF assay confirmed the parental ssDNA PLA and dSTORM data showing an increased Polα proximity with EdU in RAD52i-treated cells (Figure 7B). Surprisingly, this recruitment was not affected by MIRIN, although it was still clearly dependent on RAD51 (Figure 7B). At the 15min chase time-point, more Polα became associated with EdU-labelled DNA in RAD52 inhibited cells, as detected by SIRF, but this increased association was completely suppressed by MIRIN or RAD51i that set the PLA signals back to the wild-type values (Figure 7C).

These results suggest that defective metabolism of stalled forks in RAD52 inhibited cells promotes two types of RAD51-dependent recruitment: one independent on fork degradation by MRE11 and

another one dependent on extensive fork degradation, revealing the region of DNA labelled with EdU near which Polα could be loaded.

While it is still uncertain if BRCA2 is involved in the pro-reversal function of RAD51 at the forks, its presence is important for the strand invasion activity or for recruitment of polymerases. Thus, we questioned if inhibition of RAD52 might stimulate association of RAD51 with EdU-labelled nascent DNA exposed at the perturbed replication fork and if this was BRCA2-dependent. To this end, we performed the SIRF experiment to localise RAD51 with EdU-labelled DNA in doxycycline-inducible shBRCA2 MRC5 cells, using the 5min pulse-chase experiment described in Figure 7A. Under this scheme, we expect to observe a pool of RAD51 that is sensitive to BRCA2-depletion and that is engaged from the degraded forks and, possibly, another pool that is not affected by loss of BRCA2 since is loaded at the fork to promote its reversal. Treatment with 0.5mM HU in RAD52 mock-inhibited cells resulted in a variable number of EdU-RAD51 PLA spots, which was greatly increased upon RAD52 inhibition (Figure 7D). Doxycycline-driven BRCA2-depletion (Figure S7) did not reduce the number of RAD51 SIRF signals in wild-type cells preferentially representing recruitment of RAD51 before fork reversal (Figure 7D). In contrast, the increased EdU-RAD51 PLA spots associated to RAD52 inhibition was largely reduced by depletion of BRCA2 (Figure 7D).

Since Polα is recruited at the lagging strand and a pool of RAD51 is loaded also independently on MRE11-dependent fork degradation, we asked if all the response to loss of RAD52 might derive from a defective response to lagging strand gaps originating at perturbed replication forks. Thus, we tested if the presence of unreplicated parental ssDNA might stimulate RAD52 recruitment. To this end, we pre-treated cells with the POLA1i to block replication of the lagging strand [43] and evaluated association of RAD52 to parental ssDNA by PLA. Interestingly, pre-treatment with POLA1i increased substantially the association of RAD52 to parental ssDNA, mimicking what observed very early after HU treatment (Figure 7E).

Collectively, these results indicate that loss of RAD52 stimulates two different types of RAD51-dependent Polα recruitment in response to replication perturbation, and suggest that these responses earlier of these are linked to loss of RAD52 association with ssDNA at lagging strand discontinuities.

RAD51-Polα-dependent repriming is involved in limiting the accumulation of DNA damage in RAD52-deficient cells

Loss of RAD52 leads to a partial defect in fork restart after replication inhibition, mild genome instability and persistence of unreplicated regions in the subsequent cell cycle [15]. Having

demonstrated that inhibition of RAD52 during replication fork perturbation stimulates a peculiar, origin-independent but RAD51-dependent, engagement of Polα, we asked if this mechanism might be protective against DNA damage and genome instability accumulation.

To this aim, we evaluated the accumulation of DNA damage by the analysis of γH2AX immunostaining after replication perturbation in mock (WT) or RAD52-inhibited U2OS cells. To interfere with the Polα-mediated repriming events, we exposed cells to the low dose of POLA1i during treatment (see Figures 2E, F and S5). As shown in Figure 8A, neither RAD52i or POLA1i alone significantly increased the yield of γH2AX-positive cells in response to 0.5mM HU. However, combined with the RAD52i, treatment with POLA1i greatly enhanced the number of γH2AX-positive cells and the intensity of the staining.

Next, we evaluated if engagement of Polα-mediated repriming might counteract accumulation of chromosomal damage in cells inhibited of RAD52 by analysing GIEMSA-stained metaphase spreads. As expected, inhibition of RAD52 induced a mild increase in total chromosomal damage (Figure 8B, C). Treatment with POLA1i alone, did not induce any noticeable increase in wild-type cells while stimulated the total chromosomal damage if combined with RAD52 inhibition (Figure 8B, C). Most strikingly, combined inhibition of Polα and RAD52 did not increase the number of chromosomal breaks but greatly stimulated the number of chromosomal fusions and exchanges (Figure 8C, D). Thus, inhibition of the Polα-dependent pathway is sufficient to promote specifically the formation of complex chromosomal damage in the absence of a functional RAD52. Persistence of chromosomal damage or mitotic defects can be passed to the next generation and be visible as "scars" in terms of high 53BP1 nuclear bodies (53BP1 NBs). Thus, we evaluated the presence of 53BP1 NBs in U2OS cells recovering from perturbed replication after RAD52 inhibition or combined POLA1i and RAD52i treatment. As shown in Figure 8E, replication perturbation in the presence of the RAD52i led to some increase in the number of 53BP1 NBs as compared with non-inhibited cells. Most notably, combined treatment with RAD52i and POLA1i, significantly increased the fraction of cells with the higher number of 53BP1 NBs (Figure 8E).

Collectively, these results indicate that the RAD51-Polα pathway is a salvage mechanism that protect cells experiencing perturbed replication in the presence of a non-functional RAD52 from the accumulation of chromosomal damage and the passage to daughter cells of a damaged genome.

DISCUSSION

Here, we show that disabling the function of RAD52 is sufficient to induce accumulation of parental ssDNA gaps in response to perturbed replication. DNA gaps have been shown to frequently accumulate in cells exposed to replication stress and they can derive from either exonuclease-dependent targeting of the stalled forks, defective Okazaki fragment metabolism or from repriming events [3,44]. In human cells, repriming seems prevalently associated with the activity of PrimPol, a specialised polymerase-primase that has been shown to be activated after different kinds of replication perturbations [16,17,19,22,32,45].

Interestingly, our findings indicate that human cells can activate also PrimPol-independent repriming under certain circumstances. Indeed, loss or inhibition of RAD52-ssDNA association stimulates formation of gaps in the parental strand that are dependent on the activity of Polα, thus phenocopying what has been repeatedly reported in yeast [20,46]. This Polα-mediated formation of parental gaps is matched by a great increase in an origin-independent recruitment of Polα at parental ssDNA that supports the repriming activity rather than normal involvement in de-novo origin firing. Replication perturbation-dependent recruitment of Polα in the absence of RAD52, involves AND-1, whose recruitment is also stimulated. Since AND-1 normally assists loading and retention of Polα during lagging strand synthesis [33,47–49], it is likely that loss of RAD52 triggers a peculiar repriming activity at lagging strand as opposed to a specific or highly biased use of PrimPol that occurs at the leading strand [21]. Of note, some PrimPol recruitment still occurs in the absence of RAD52 but it is not stimulated upon replication arrest significantly, as observed in RAD52-proficient cells and much more in BRCA2-depleted cells.

Our data indicate that, in RAD52-deficient cells, the Polα recruitment and Polα-stimulated accumulation of parental ssDNA occur downstream fork reversal as they are strongly reduced by downregulation of SMARCAL1 or ZRANB3, two of the critical enzymes involved in fork remodelling [9]. This is paralleled by strong dependency on MRE11 activity suggesting that most if not all of the Polα-mediated repriming occurring in RAD52-deficient cells is a response to extensive fork degradation, which happens when RAD52 is inhibited [15]. These findings differentiate such Polα-mediated repriming from that mediated by PrimPol, which acts in a parallel pathway with the fork reversal [16]. However, why loss of RAD52 or BRCA2 stimulates fork degradation but does not stimulate the same repriming pathway? In BRCA2-deficient cells, degradation of the reversed fork is followed by endonucleolytic cleavage by the MUS81/EME2 complex and break-induced replication to promote restart of DNA synthesis [36]. Loss of RAD52 promotes fork degradation but does not induce fork cleavage because RAD52 also regulates MUS81-dependent DSBs [37]. Our

findings indicate that co-depletion of MUS81 and BRCA2 is sufficient to stimulate Polα recruitment at parental ssDNA following replication perturbation, recapitulating what happens when RAD52 is inhibited. Depletion of MUS81 in BRCA2-deficient cells leads to extended fork degradation, which is the same observed in cells inhibited of RAD52 during replication arrest [15]. This suggest that extended degradation, which might reset the reversed fork, could also promote repriming on both DNA strands as shown in yeast [20].

We find that Polα-dependent ssDNA gaps and Polα recruitment under perturbed replication are dependent on RAD51 especially in the absence of RAD52. Moreover, our data show that Polα and RAD51 interacts under these conditions. RAD51 is important for fork restart and has been previously shown to interact with Polα for its localisation at the fork [39]. Furthermore, it has been reported that RAD51 and MRE11 can stimulate an origin-independent re-loading of the replisome at collapsed replication forks [50]. However, our data indicate that RAD51-dependent Polα recruitment occurs, in the absence of fork collapse, downstream fork reversal/degradation and not before of it also to avoid fork remodelling [39]. Our findings also show that even a small reduction in the amount of RAD51 is sufficient to interfere with Polα recruitment and gap accumulation. Since only the extensive RAD51 nucleation associated to strand invasion or fork protection is sensitive to even limited depletion [14] and inhibition of RAD52 *per se* induces fork deprotection in wild-type cells [15], this evidence might suggest that Polα is recruited downstream a strand-invasion event. Consistent with this, inhibition of RAD52 leads to an increased and BRCA2-dependent recruitment of RAD51 at the nascent DNA left behind the perturbed forks. In yeast, mutations leading to extensive processing of reversed forks can stimulate either Polα repriming or template-switching and repriming post strand invasion, which might be dependent on Polα primase [20,51]. Thus, our observations could support a similar mechanism also in human cells, demonstrating that PrimPol is not the only available repriming mechanism. Of note, we find that RAD52 recruitment is stimulated by a treatment inducing a biased discontinuity in the lagging strand. This result might be consistent with the observed role of RAD52 at the fork in preventing unscheduled activity of SMARCAL1 [15], which should be only loaded at leading strand to establish productive intermediates for subsequent replication restart [52]. From this point of view, inhibition of RAD52 might stimulate an early recruitment of Polα that is not dependent on MRE11 but still requires RAD51 at lagging strand and a late MRE11-dependent Polα recruitment that originates from template switching downstream nucleolytic reset of the reversed fork (Figure 8F). Alternatively, the RAD51-dependent Polα recruitment might always take place at lagging strand before and after the extensive fork degradation by MRE11 (Figure 8F). Interestingly, it has been recently reported that also Polθ can be

recruited at the lagging strand to fill-in template gaps in the absence of RAD51 [53]. Thus multiple mechanism might contribute to prevent excessive fork reversal and accumulation of template gaps.

We previously demonstrated that inhibition of RAD52, although determining a striking fork degradation phenotype, does not impair as strongly fork restart [15]. This was not unexpected since fork degradation is not associated to a significant decrease in fork restart also in BRCA2-deficient cells [54]. However, in BRCA2-deficient cells, restart has been proposed to occur through at least two pathways: BIR and repriming by PrimPol [31,36]. A mild inhibition of Polα limits fork restart in the absence of RAD52, indicating that when forks get degraded but BIR cannot be engaged, cells have another additional mechanism to channel extensively degraded forks into a "secondary" restart pathway. This "secondary" pathway is however important to limit DNA damage in response to perturbed replication. Indeed, the mild inhibition of Polα not only reduces fork restart but strikingly increases signs of replication stress, such as γH2AX foci and chromosomal damage. This backup pathway might also contribute to explain why RAD52 knock-down in humans does not generate a strong phenotype [11].

Altogether, our findings may be summarized in the model proposed in Figure 8F. Replication perturbation, by uncoupling unwinding from DNA synthesis, stimulates the recruitment of RAD52 at the fork, most probably at the lagging strand. Recruitment of RAD52 functions as a gatekeeper limiting unscheduled and perhaps "error-prone" engagement of SMARCAL1, as previously demonstrated [15]. In the absence of RAD52, on one hand, BRCA2 and RAD51 promotes Polα recruitment at the lagging strand gap, with or without intervention of an unknown exonuclease, while, on the other hand, the reversed forks are degraded eventually leading to fork reset and parental DNA exposure. The two events might be interlinked. Another round of BRCA2 and RAD51-dependent Polα recruitment might occur at the reset fork directly or downstream strand-invasion by RAD51. Currently, we cannot give clues on the identity of the strand initiating template switch (leading or lagging). This mechanism would support fork restart and limit DNA damage that otherwise accumulates upon replication perturbation in the absence of RAD52 (Figure 8).

RAD52 can be found mutated in cancer [55]. It will be interesting to assess if cancer-related mutations disable the gatekeeper role of RAD52 predisposing cells to use Polα-mediated repriming and becoming hypersensitive to inhibitors of Polα. Moreover, RAD52 loss or inhibition is extremely synthetic sick with loss of BRCA2 or the checkpoint [37,56,57]. The interaction between RAD51 and Polα has been preliminary mapped in the Xenopus model system [39], and separation of function would be a useful tool to determine if this genetic relationship also correlates with an inability to perform RAD51-Polα-mediated repriming at distressed forks.

LIMITATIONS OF THE STUDY

In this study, we report an increase in ssDNA gaps upon RAD52 inhibition that is dependent on Polα and occurs downstream fork reversal and extensive fork degradation in the absence of MUS81-dependent DSBs. Although we could clearly observe RAD52 engaged upon stimulation of lagging strand gap formation and that the Polα recruitment and ssDNA gap accumulation was dependent on RAD51 in the absence of RAD52, we could not determine exactly if this is exclusively due to RAD51 engagement at lagging strand discontinuities or template switching from degraded leading strand. This is because of the essential role of RAD51 in both pathways and in the absence of separation of function mutants. In addition, we cannot rule out that template switching is initiated from a lagging strand gap because is impossible to discriminate between EdU incorporation at the leading vs. lagging strand. Thus, we could not give conclusive information on the localisation of gaps. Moreover, the essential role of Polα prevented reliable genetic experiments using RNAi. Further investigation using RAD51 or Polα mutants abrogating this protein-protein interaction or the identification of separation of function mutations in this pathway will be required to clarify this point.

MATERIALS AND METHODS

Cell lines and culture conditions

The MRC5SV40 and human osteosarcoma cell line (U2OS) were maintained in Dulbecco's modified Eagle's medium (DMEM, Euroclone) supplemented with 10% fetal bovine serum (Euroclone) and incubated at 37 °C in a humidified 5% CO2 atmosphere. MRC5SV40 -/- PrimPol was a kind gift from Professor Aidan Doherty of Sussex University. MRC5 -/- MUS81 was obtained with the Crispr/Cas9 system by using two Alt-R® Crispr-Cas9 gRNA (Hs.Cas9.MUS81.1.AA and Hs.Cas9.MUS81.1.AB) and successively transfected with the WT protein. MRC5 shBRCA2 or U2OS shSMARCAL1 were transfected with lentiviruses expressing the shSMARCAL1 or shBRCA2 cassette under the control of a doxycycline (Dox)-regulated promoter, at 0.5 of multiplicity of infection (MOI) (Dharmacon SmartVector inducible lentivirus, sequence code: V3SH11252-227970177 (shSMARCAL) and V3SH7669-226099147 (shBRCA2). After puromycin selection at 300 ng/ml, a single clone was selected and used throughout the study. SMARCAL1 overexpressing U2OS was obtained by the transfection of U2OS WT cells with the inducible PiggyBac/Transposase system, in a proportion of 9:1 [35]. Cell lines were routinely tested for mycoplasma contamination and maintained in cultures for no more than one month.

Oligos and plasmids

siRNA

WDHD1 (AND-1)	Sigma Aldrich MISSION esiRNA #EHU134421
ZRANB3	Dharmacon siGENOME siRNA D-010025-03-005 cat # 84083
MUS81	Qiagen FlexiTube siRNA cat # SI04300877 oligo #6
BRCA2	Dharmacon ON TARGET PLUS SMARTpool siRNA #SO-2994934G
RAD51 (J11)	Dharmacon ON TARGET PLUS siRNA #SO-2960294G

Plasmids

peGFP-PrimPol WT	Bailey et al., 2019
PiggyBac-SMARCAL1 WT	Pugliese et al., 2019
pFLAG-MUS81 WT	Palma et al., 2018

Transfections

All the siRNAs were transfected using Interferin® (Polyplus) 48 h before to perform experiments. WDHD1 siRNA was used at 10 nM. RAD51 siRNA (J11) was used at 2 and 20 pmol. MUS81 and BRCA2 siRNAs were used at 25 nM. ZRANB3 siRNA was used at 50 nM. The peGFP-PrimPol, PiggyBac-SMARCAL1 and pFLAG-MUS81 were transfected in cell lines using NeonTM transfection system (Invitrogen) 48 h prior to perform experiments.

Chemicals

HU (Sigma-Aldrich) was added to culture medium at 2 mM or 0.5 mM from a 200 mM stock solution prepared in Phosphate-buffer saline solution (PBS 1X) to induce DNA replication arrest or slowing. RAD52 inhibitor, Epigallocatechin (EGC - Sigma-Aldrich) was dissolved in DMSO at 100 mM and used at 50 µM. The B02 compound (Selleck), an inhibitor of RAD51 activity, was used at 27 µM. CDC7i (XL413, Selleck) was dissolved in sterile water and used 10 µM. Doxycycline (Sigma-Aldrich) was dissolved in DMSO and used 1µ/ml. MIRIN, the inhibitor of MRE11 exonuclease activity (Calbiochem), was used at 50 µM. Polα inhibitor (ST1926 – Sigma-Aldrich) was dissolved in DMSO and used at the concentrations reported on the experiments. S1 nuclease (Invitrogen cat # 18001016) was diluted 1/100 in S1 buffer and used at 20 U/ml. CldU (Sigma-Aldrich) was dissolved in sterile water as a 200 mM stock solution and used at 50 µM. IdU (Sigma-Aldrich) was dissolved in sterile DMEM as a stock solution 2.5 mM and used at 100 for ssDNA and PLA assays or 250 µM for fibers assay. 5-ethynyl-2'-deoxyuridine (EdU) (Sigma-Aldrich) Was dissolved in DMSO and used at 10 µM for EdU incorporation assay or 100 µM for SIRF assay.

Western blot analysis

Western blots were performed using standard methods. Blots were incubated with primary antibodies against: anti-GFP (Santa Cruz Biotechnology, 1:500), anti-MUS81 (Santa Cruz Biotechnology, 1:1000), anti-LAMIN B1 (Abcam, 1:10,000), anti-GAPDH (Millipore, 1:5000), anti-RAD51 (Abcam 1:10,000), anti-SMARCAL1 (Bethyl 1:1500), anti-ZRANB3 (Proteintech 1:1000), anti-BRCA2 (Bethyl 1:5000), anti-POLA1 (Polα - Bethyl, 1:500), anti-WDHD1 (Novus Biologicals, 1:1000). After incubations with horseradish peroxidase-linked secondary antibodies (Jackson ImmunoResearch, 1:20,000), the blots were developed using the chemiluminescence detection kit ECL-Plus (Amersham) according to the manufacturer's instructions. Quantification was performed on blot acquired by ChemiDoc XRS+ (Bio-Rad) using Image Lab software, the normalization of the protein content was done through LAMIN B1 or GAPDH immunoblotting.

Chromatin isolation

After the treatments, cells (4 × 106 cells/ml) were resuspended in buffer A (10 mM HEPES, [pH 7.9], 10 mM KCl, 1.5 mM MgCl2, 0.34 M sucrose, 10% glycerol, 1 mM DTT, 50 mM sodium fluoride, protease inhibitors [Roche]). Then was added Triton X-100 at a final concentration of 0.1% and the cells were incubated for 5 min on ice. Nuclei were collected in pellet by low-speed centrifugation (4 min, 1300 × g, 4 °C) and washed once in buffer A. Nuclei were then lysed in buffer B (3 mM EDTA, 0.2 mM EGTA, 1 mM DTT, protease inhibitors) for 10 min on ice. Insoluble chromatin was collected by centrifugation (4 min, 1700 × g, 4 °C), washed once in buffer B + 50 mM NaCl, and centrifuged again under the same conditions. The final chromatin pellet was resuspended in 2X Laemmli buffer and sonicated for 15 s in a Tekmar CV26 sonicator using a microtip at 50% amplitude.

EdU incorporation assay

U2OS were treated with 10 µM EdU 10 min before giving the treatment with ST1926 for 30 min at the indicated concentrations. After the treatment, cells were permeabilized with 0.5% TritonX-100 in PBS 1X for 10 minutes on ice, then fixed with 3% PFA, 2% sucrose in PBS 1X at room temperature (RT) for 15 min. For the EdU detection was applied the Click-iT™ EdU Alexa Fluor™ 488 Imaging Kit (Invitrogen) for 30 minutes at RT. The reagents for the Click-iT™ reaction were diluted according to the manufacturer's instructions. Nuclei were examined with Eclipse 80i Nikon Fluorescence Microscope, equipped with a Virtual Confocal (ViCo) system and foci were scored at 40X magnification. Quantification was carried out using the ImageJ software.

Detection of ssDNA by native IdU assay

To detect parental ssDNA, cells were labelled for 20 hours with 50 µM IdU (Sigma-Aldrich), released in fresh DMEM for 2 hours, then treated as indicated. For immunofluorescence, cells were washed with PBS 1X, permeabilized with 0.5% Triton X-100 for 10 min at 4 °C and fixed in 3% PFA, 2% sucrose in PBS 1X. Fixed cells were then incubated with mouse anti-IdU antibody (Becton Dickinson, 1:80) for 1 h at 37 °C in 1% BSA/PBS, followed by species-specific fluorescein-conjugated secondary antibodies (Alexa Fluor 488 Goat Anti-Mouse IgG (H + L), highly cross-adsorbed—Life Technologies). Slides were analysed with Eclipse 80i Nikon Fluorescence Microscope, equipped with a Virtual Confocal (ViCo) system. For each time point, at least 100 nuclei were analysed. Quantification was carried out using the ImageJ software.

In situ PLA assay for ssDNA–protein interaction

The in situ PLA (Duolink®, Sigma-Aldrich) or NaveniFlex (Navinci Diagnostics) was performed according to the manufacturer's instructions. For parental ssDNA-protein interaction, cells were labelled with 100 μM IdU for 20 hours and then released in fresh medium for 2 hours. After treatment, cells were permeabilized with 0.5% Triton X-100 for 10 min at 4 °C, fixed with 3% PFA/2% sucrose in PBS 1X for 10 min and then blocked in 3% BSA/PBS for 15 min. After washing with PBS, cells were incubated with the two relevant primary antibodies. The primary antibodies used were as follows: mouse monoclonal anti-RAD51 (GeneTex, 1:150), mouse monoclonal anti-IdU (Becton Dickinson, 1:50), rabbit polyclonal anti-Polα (Bioss, 1:50), rabbit polyclonal anti-GFP (Invitrogen 1:150), rabbit anti-WDHD1 (Novus Biologicals, 1:50), rabbit anti-RAD52 (Aviva, 1:150). The negative controls were obtained by using only one primary antibody. Samples were incubated with secondary antibodies conjugated with PLA probes MINUS and PLUS: the PLA probe anti-mouse PLUS and anti-rabbit MINUS (or NaveniFlex equivalent). The incubation with all antibodies was accomplished in a humidified chamber for 1 h at 37 °C. Next, the PLA probes MINUS and PLUS were ligated using two connecting oligonucleotides to produce a template for rolling-cycle amplification. After amplification, the products were hybridized with red fluorescence-labelled oligonucleotide. Samples were mounted in Prolong Gold anti-fade reagent with DAPI (blue). Images were acquired randomly using Eclipse 80i Nikon Fluorescence Microscope, equipped with a Virtual Confocal (ViCo) system.

Single-cell Assay for in situ Protein Interaction with Nascent DNA (SIRF)

Exponential growing cells were seeded onto microscope chamber slide. The day of experiment, cells were incubated with 100 μM EdU for 20 min and treated as indicated. After treatment, cells were pre-extracted in 0.5% TritonX-100 for 5 min on ice and fixed with 3% PFA, 2% sucrose in PBS 1X for 15 min at RT. Cells were then blocked in 3% BSA/PBS for 15 min. For the EdU detection was applied the Click-iT™ EdU Alexa Fluor™ Imaging Kit (Invitrogen) using 5mM Biotin-Azide for 30 minutes at RT. The primary antibodies used were as follows: mouse monoclonal anti-RAD51 (GeneTex, 1:150), rabbit polyclonal anti-Polα (Bioss, 1:50), mouse anti-biotin (Invitrogen, 1:50) rabbit anti-biotin (Abcam, 1:50). The negative controls were obtained by using only one primary antibody. Samples were incubated with secondary antibodies conjugated with PLA probes MINUS and PLUS: the PLA probe anti-mouse PLUS and anti-rabbit MINUS (Duolink®, Sigma-Aldrich). The incubation with all antibodies was accomplished in a humidified chamber for 1 h at 37 °C. Next, the PLA probes MINUS and PLUS were ligated using two connecting oligonucleotides to produce a template for rolling-cycle amplification. After

amplification, the products were hybridized with red fluorescence-labelled oligonucleotide. Samples were mounted in Prolong Gold anti-fade reagent with DAPI (blue). Images were acquired randomly using Eclipse 80i Nikon Fluorescence Microscope, equipped with a Virtual Confocal (ViCo) system.

Single-Molecule Localisation Microscopy

U2OS cells were treated as indicated in the experimental scheme. After the treatment, cells were fixed and immunofluorescence was performed as described by Whelan & Rothenberg, 2021. EdU was detected with the Click-iT™ EdU Alexa Fluor™ Imaging Kit (Invitrogen) for 30 minutes at RT. Coverslips with fixed cells were stored for up to 1 week at 4 °C prior to dSTORM imaging. The fixed cells on coverslips were mounted onto concave slides and dSTORM imaging B3 buffer from Oxford Nanoimaging (ONI, PN #900-00004) was added before imaging. A commercial TIRF microscope (Nanoimager S Mark IIB from ONI, https://oni.bio) with lasers of 405 nm/150 mW, 488 nm/1 W, 561 nm/1 W, and 640 nm/1 W was used to acquire data. Briefly, fluorophore emission was collected by an oil immersion 100x/1.45NA objective and images were acquired at 30 ms exposure time using a Hamamatsu ORCA-Flash4.0 V3 Digital sCMOS camera. The reconstruction of the super-resolution image was conducted by NimOS software from ONI. Localization data were then analyzed using the ONI-CODI platform for drift correction, filtering, clustering, and counting.

DNA fibers analysis

Fibers assay using S1 nuclease was performed as indicated by Quinet et al., 2017. Briefly, cells were pulse-labelled with 50 µM CldU and then labelled with 250 µM IdU with or without treatment, as reported in the experimental schemes. At end of treatment, cells were permeabilized with CSK buffer (100 mM NaCl, 10 mM PIPES pH 6.8, 1M EGTA, 3 mM MgCl2, 300 mM sucrose, 0.5% Triton X-100) for 10 min at RT, then were washed with PBS 1X and S1 nuclease buffer (30 mM sodium acetate, 10 mM zinc acetate, 5% glycerol, 50 mM NaCl) prior to add +/- S1 nuclease for 30 min at 37 °C in a humidified chamber. Cells were washed with S1 buffer then scraped with 0.1% BSA/PBS and collected pellets were used to perform fibers spreading. DNA fibers were spread out as described by Iannascoli et al., 2015. For immunodetection of labelled tracks, the following primary antibodies were used: rat anti-CldU/BrdU (Abcam 1:50) and mouse anti-IdU/BrdU (Becton Dickinson 1:10). Images were acquired randomly from fields with untangled fibers using Eclipse 80i Nikon Fluorescence Microscope, equipped with a Virtual Confocal (ViCo) system. The length of labelled tracks was measured using the Image-Pro-Plus 6.0 software.

Chromosomal aberrations

MRC5SV40 cells were treated with HU 2 mM, with or without RAD52 inhibitor and/or Polα inhibitor, left at 37 °C for 4 hours, then allowed to recover in fresh medium for additional 24 hours. Cell cultures were incubated with colcemid (0.2 μg/ml) at 37 °C for 3 hours until harvesting. Cells for metaphase preparations were collected and prepared as previously reported by Iannascoli et al., 2015. For each condition, at least 50 chromosomes were examined and chromosomal damage scored at 100× magnification.

Statistical analysis

All the data are presented as means of at least two pooled independent experiments. Statistical analyses were performed by one-sided analysis of variance (ANOVA) or Mann–Whitney test using the built-in tools in Prism 9 (GraphPad Inc.). $P < 0.5$ was considered as significant. Statistical significance was always denoted as follow: ns = not significant; *$P < 0.5$; **$P < 0.01$; ***$P < 0.01$; ***$P < 0.001$. Specific statistical analyses are reported in the relevant legend.

ACKNOWLEDGMENTS

We thank Prof. Aidan Doherty for PrimPol KO cells and GFP-PrimPol expressing plasmid. We thank Dr. Patricia Kannouche for the MRC5SV40 cells. We want to thank Prof. Maria Spies and Luca Pellegrini for helpful discussion and advise. This work was supported by NIH-NCI grant (grant n. R01CA232425-A1) and by investigator grants from Associazione Italiana per la Ricerca sul Cancro (AIRC) to P.P. (IG n. 21428) and to A.F. (IG n. 19971).

AUTHORS CONTRIBUTION

L.D.B performed all experiments to analyse formation and mechanism of Polα-dependent parental DNA gaps using RAD52i. E.M. performed analysis of parental ssDNA formation in RAD52 knockdown cells and contributed to S1 DNA fiber assay. F.A.A. performed dSTORM experiments. P.V. performed the analyses of chromosome damage. All authors contributed to design experiments and analyze data. P.P and A.F. designed experiments, analysed data and supervised the project. L.D.B. contributed to write results. P.P. wrote the paper. All authors contributed to revise the paper.

CONFLICT OF INTEREST

The authors declare to do not have any conflict of interest

REFERENCES

1. Flynn, R.L., and Zou, L. (2011). ATR: A master conductor of cellular responses to DNA replication stress. Trends Biochem. Sci. *36*, 133–140. 10.1016/j.tibs.2010.09.005.
2. Zeman, M.K., and Cimprich, K.A. (2014). Causes and consequences of replication stress. Nat. Cell Biol. *16*, 2–9. 10.1038/ncb2897.
3. Thakar, T., and Moldovan, G. (2021). The emerging determinants of replication fork stability. Nucleic Acids Res. *49*, 7224–7238. 10.1093/nar/gkab344.
4. Franchitto, A., and Pichierri, P. (2014). Replication fork recovery and regulation of common fragile sites stability. Cell. Mol. Life Sci. *71*, 4507–4517. 10.1007/s00018-014-1718-9.
5. Pasero, P., and Vindigni, A. (2017). Nucleases Acting at Stalled Forks: How to Reboot the Replication Program with a Few Shortcuts. Annu. Rev. Genet. *51*, 477–499. 10.1146/annurev-genet-120116-024745.
6. Berti, M., Cortez, D., and Lopes, M. (2020). The plasticity of DNA replication forks in response to clinically relevant genotoxic stress. Nat. Rev. Mol. Cell Biol. *21*, 633–651. 10.1038/s41580-020-0257-5.
7. Neelsen, K.J., and Lopes, M. (2015). Replication fork reversal in eukaryotes: from dead end to dynamic response. Nat. Rev. Mol. Cell Biol. *16*, 207–220. 10.1038/nrm3935.
8. McGlynn, P., and Lloyd, R.G. (2002). Genome stability and the processing of damaged replication forks by RecG. Trends Genet. *18*, 413–419. 10.1016/S0168-9525(02)02720-8.
9. Joseph, S.A., Taglialatela, A., Leuzzi, G., Huang, J.-W., Cuella-Martin, R., and Ciccia, A. (2020). Time for remodeling: SNF2-family DNA translocases in replication fork metabolism and human disease. DNA Repair *95*, 102943. 10.1016/j.dnarep.2020.102943.
10. Kolinjivadi, A.M., Sannino, V., de Antoni, A., Técher, H., Baldi, G., and Costanzo, V. (2017). Moonlighting at replication forks - a new life for homologous recombination proteins BRCA1, BRCA2 and RAD51. FEBS Lett., 1–18. 10.1002/1873-3468.12556.
11. Malacaria, E., Honda, M., Franchitto, A., Spies, M., and Pichierri, P. (2020). Physiological and Pathological Roles of RAD52 at DNA Replication Forks. Cancers *12*, 402. 10.3390/cancers12020402.
12. Leuzzi, G., Marabitti, V., Pichierri, P., and Franchitto, A. (2016). WRNIP1: A new guardian of genome integrity at stalled replication forks. Mol. Cell. Oncol. *3*, e1215777. 10.1080/23723556.2016.1215777.
13. Couch, F.B., Bansbach, C.E., Driscoll, R., Luzwick, J.W., Glick, G.G., Bétous, R., Carroll, C.M., Jung, S.Y., Qin, J., Cimprich, K. a., et al. (2013). ATR phosphorylates SMARCAL1 to prevent replication fork collapse. Genes Dev. *27*, 1610–1623. 10.1101/gad.214080.113.
14. Bhat, K.P., Krishnamoorthy, A., Dungrawala, H., Garcin, E.B., Modesti, M., and Cortez, D. (2018). RADX Modulates RAD51 Activity to Control Replication Fork Protection. Cell Rep. *24*, 538–545. 10.1016/j.celrep.2018.06.061.
15. Malacaria, E., Pugliese, G.M., Honda, M., Marabitti, V., Aiello, F.A., Spies, M., Franchitto, A., and Pichierri, P. (2019). Rad52 prevents excessive replication fork reversal and protects from nascent strand degradation. Nat. Commun. *10*, 1–19. 10.1038/s41467-019-09196-9.
16. Quinet, A., Tirman, S., Jackson, J., Šviković, S., Lemaçon, D., Carvajal-Maldonado, D., González-Acosta, D., Vessoni, A.T., Cybulla, E., Wood, M., et al. (2020). PRIMPOL-Mediated

Adaptive Response Suppresses Replication Fork Reversal in BRCA-Deficient Cells. Mol. Cell *77*, 461-474.e9. 10.1016/j.molcel.2019.10.008.

17. Tirman, S., Quinet, A., Wood, M., Meroni, A., Cybulla, E., Jackson, J., Pegoraro, S., Simoneau, A., Zou, L., and Vindigni, A. (2021). Temporally distinct post-replicative repair mechanisms fill PRIMPOL-dependent ssDNA gaps in human cells. Mol. Cell *81*, 4026-4040.e8. 10.1016/J.MOLCEL.2021.09.013.
18. Bai, G., Kermi, C., Stoy, H., Schiltz, C.J., Bacal, J., Zaino, A.M., Hadden, M.K., Eichman, B.F., Lopes, M., and Cimprich, K.A. (2020). HLTF Promotes Fork Reversal, Limiting Replication Stress Resistance and Preventing Multiple Mechanisms of Unrestrained DNA Synthesis. Mol. Cell *78*, 1237-1251.e7. 10.1016/j.molcel.2020.04.031.
19. Bianchi, J., Rudd, S.G., Jozwiakowski, S.K., Bailey, L.J., Soura, V., Taylor, E., Stevanovic, I., Green, A.J., Stracker, T.H., and Lindsay, H.D. (2013). Primpol bypasses UV photoproducts during eukaryotic chromosomal DNA replication. Mol. Cell *52*, 566–573. 10.1016/j.molcel.2013.10.035.
20. Fumasoni, M., Zwicky, K., Vanoli, F., Lopes, M., and Branzei, D. (2015). Error-Free DNA Damage Tolerance and Sister Chromatid Proximity during DNA Replication Rely on the Polα/Primase/Ctf4 Complex. Mol. Cell *57*, 812–823. 10.1016/j.molcel.2014.12.038.
21. Guilliam, T., and Doherty, A. (2017). PrimPol—Prime Time to Reprime. Genes *8*, 20. 10.3390/genes8010020.
22. Piberger, A.L., Bowry, A., Kelly, R.D.W., Walker, A.K., González-Acosta, D., Bailey, L.J., Doherty, A.J., Méndez, J., Morris, J.R., Bryant, H.E., et al. (2020). PrimPol-dependent single-stranded gap formation mediates homologous recombination at bulky DNA adducts. Nat. Commun. *11*, 1–14. 10.1038/s41467-020-19570-7.
23. Branzei, D., and Szakal, B. (2016). DNA damage tolerance by recombination: Molecular pathways and DNA structures. DNA Repair *44*, 68–75. 10.1016/j.dnarep.2016.05.008.
24. Quinet, A., Tirman, S., Cybulla, E., Meroni, A., and Vindigni, A. (2021). To skip or not to skip: choosing repriming to tolerate DNA damage. Mol. Cell, 1–10. 10.1016/j.molcel.2021.01.012.
25. Cortez, D. (2019). Replication-Coupled DNA Repair. Mol. Cell *74*, 866–876. 10.1016/j.molcel.2019.04.027.
26. Hengel, S.R., Spies, M.A., and Spies, M. (2017). Small-Molecule Inhibitors Targeting DNA Repair and DNA Repair Deficiency in Research and Cancer Therapy. Cell Chem. Biol. *24*, 1101–1119. 10.1016/j.chembiol.2017.08.027.
27. Iannascoli, C., Palermo, V., Murfuni, I., Franchitto, A., and Pichierri, P. (2015). The WRN exonuclease domain protects nascent strands from pathological MRE11/EXO1-dependent degradation. Nucleic Acids Res. *43*, 9788–9803. 10.1093/nar/gkv836.
28. Peng, M., Cong, K., Panzarino, N.J., Nayak, S., Calvo, J., Deng, B., Zhu, L.J., Morocz, M., Hegedus, L., Haracska, L., et al. (2018). Opposing Roles of FANCJ and HLTF Protect Forks and Restrain Replication during Stress. Cell Rep. *24*, 3251–3261. 10.1016/j.celrep.2018.08.065.
29. Quinet, A., Carvajal-Maldonado, D., Lemacon, D., and Vindigni, A. (2017). Chapter Three – DNA Fiber Analysis: Mind the Gap! In Methods in Enzymology, pp. 55–82. 10.1016/bs.mie.2017.03.019.
30. Cong, K., Peng, M., Kousholt, A.N., Lee, W.T.C., Lee, S., Nayak, S., Krais, J., VanderVere-Carozza, P.S., Pawelczak, K.S., Calvo, J., et al. (2021). Replication gaps are a key determinant

of PARP inhibitor synthetic lethality with BRCA deficiency. Mol. Cell *81*, 3128-3144.e7. 10.1016/j.molcel.2021.06.011.

31. Kang, Z., Fu, P., Alcivar, A.L., Fu, H., Redon, C., Foo, T.K., Zuo, Y., Ye, C., Baxley, R., Madireddy, A., et al. (2021). BRCA2 associates with MCM10 to suppress PRIMPOL-mediated repriming and single-stranded gap formation after DNA damage. Nat. Commun. 2021 121 *12*, 1–12. 10.1038/s41467-021-26227-6.
32. Bailey, L.J., Bianchi, J., and Doherty, A.J. (2019). PrimPol is required for the maintenance of efficient nuclear and mitochondrial DNA replication in human cells. Nucleic Acids Res. *47*, 4026–4038. 10.1093/nar/gkz056.
33. Zhu, W. (2007). Mcm10 and And-1/CTF4 recruit DNA polymerase alpha to chromatin for initiation of DNA replication. Genes Dev *21*, 2288–2299. 10.1101/gad.1585607.
34. Ercilla, A., Benada, J., Amitash, S., Zonderland, G., Baldi, G., Somyajit, K., Ochs, F., Costanzo, V., Lukas, J., and Toledo, L. (2020). Physiological Tolerance to ssDNA Enables Strand Uncoupling during DNA Replication. Cell Rep. *30*, 2416-2429.e7. 10.1016/j.celrep.2020.01.067.
35. Pugliese, G.M., Salaris, F., Palermo, V., Marabitti, V., Morina, N., Rosa, A., Franchitto, A., and Pichierri, P. (2019). Inducible SMARCAL1 knockdown in iPSC reveals a link between replication stress and altered expression of master differentiation genes. Dis. Model. Mech. *12*, dmm039487. 10.1242/dmm.039487.
36. Lemaçon, D., Jackson, J., Quinet, A., Brickner, J.R., Li, S., Yazinski, S., You, Z., Ira, G., Zou, L., Mosammaparast, N., et al. (2017). MRE11 and EXO1 nucleases degrade reversed forks and elicit MUS81-dependent fork rescue in BRCA2-deficient cells. Nat. Commun. *8*, 860. 10.1038/s41467-017-01180-5.
37. Murfuni, I., Basile, G., Subramanyam, S., Malacaria, E., Bignami, M., Spies, M., Franchitto, A., and Pichierri, P. (2013). Survival of the Replication Checkpoint Deficient Cells Requires MUS81-RAD52 Function. PLoS Genet. *9*, e1003910. 10.1371/journal.pgen.1003910.
38. Blandino, F., Malacaria, E., Pugliese, G.M., Franchitto, A., and Pichierri, P. (2022). Phosphorylation Status of Mus81 Is a Modifier of Olaparib Sensitivity in Brca2-Deficient Cells. 2022.08.13.503764. 10.1101/2022.08.13.503764.
39. Kolinjivadi, A.M., Sannino, V., De Antoni, A., Zadorozhny, K., Kilkenny, M., Técher, H., Baldi, G., Shen, R., Ciccia, A., Pellegrini, L., et al. (2017). Smarcal1-Mediated Fork Reversal Triggers Mre11-Dependent Degradation of Nascent DNA in the Absence of Brca2 and Stable Rad51 Nucleofilaments. Mol. Cell *67*, 867-881.e7. 10.1016/j.molcel.2017.07.001.
40. Adolph, M.B., Mohamed, T.M., Balakrishnan, S., Xue, C., Morati, F., Modesti, M., Greene, E.C., Chazin, W.J., and Cortez, D. (2021). RADX controls RAD51 filament dynamics to regulate replication fork stability. Mol. Cell *81*, 1074-1083.e5. 10.1016/j.molcel.2020.12.036.
41. Zellweger, R., Dalcher, D., Mutreja, K., Berti, M., Schmid, J.A., Herrador, R., Vindigni, A., and Lopes, M. (2015). Rad51-mediated replication fork reversal is a global response to genotoxic treatments in human cells. J. Cell Biol. *208*, 563–579. 10.1083/jcb.201406099.
42. Xu, Y., Ning, S., Wei, Z., Xu, R., Xu, X., Xing, M., Guo, R., and Xu, D. (2017). 53BP1 and BRCA1 control pathway choice for stalled replication restart. eLife *6*, e30523. 10.7554/eLife.30523.

43. Lukac, D., Machacova, Z., and Moudry, P. (2022). Emetine blocks DNA replication via proteosynthesis inhibition not by targeting Okazaki fragments. Life Sci. Alliance *5*, e202201560. 10.26508/lsa.202201560.
44. Cong, K., and Cantor, S.B. (2022). Exploiting replication gaps for cancer therapy. Mol. Cell *82*, 2363–2369. 10.1016/j.molcel.2022.04.023.
45. González-Acosta, D., Blanco-Romero, E., Ubieto-Capella, P., Mutreja, K., Míguez, S., Llanos, S., García, F., Muñoz, J., Blanco, L., Lopes, M., et al. (2021). PrimPol-mediated repriming facilitates replication traverse of DNA interstrand crosslinks. EMBO J., 1–17. 10.15252/embj.2020106355.
46. Taylor, M.R.G., and Yeeles, J.T.P. (2018). The Initial Response of a Eukaryotic Replisome to DNA Damage. Mol. Cell *70*, 1067-1080.e12. 10.1016/j.molcel.2018.04.022.
47. Abe, T., Kawasumi, R., Giannattasio, M., Dusi, S., Yoshimoto, Y., Miyata, K., Umemura, K., Hirota, K., and Branzei, D. (2018). AND-1 fork protection function prevents fork resection and is essential for proliferation. Nat. Commun. *9*, 3091. 10.1038/s41467-018-05586-7.
48. Gambus, A., van Deursen, F., Polychronopoulos, D., Foltman, M., Jones, R.C., Edmondson, R.D., Calzada, A., and Labib, K. (2009). A key role for Ctf4 in coupling the MCM2-7 helicase to DNA polymerase α within the eukaryotic replisome. EMBO J. *28*, 2992–3004. 10.1038/emboj.2009.226.
49. Errico, A., Cosentino, C., Rivera, T., Losada, A., Schwob, E., Hunt, T., and Costanzo, V. (2009). Tipin/Tim1/And1 protein complex promotes Pol alpha chromatin binding and sister chromatid cohesion. EMBO J. *28*, 3681–3692. 10.1038/emboj.2009.304.
50. Hashimoto, Y., Puddu, F., and Costanzo, V. (2011). RAD51- and MRE11-dependent reassembly of uncoupled CMG helicase complex at collapsed replication forks. Nat. Struct. Mol. Biol. *19*, 17–24. 10.1038/nsmb.2177.
51. Cotta-Ramusino, C., Fachinetti, D., Lucca, C., Doksani, Y., Lopes, M., Sogo, J., and Foiani, M. (2005). Exo1 processes stalled replication forks and counteracts fork reversal in checkpoint-defective cells. Mol. Cell *17*, 153–159. 10.1016/j.molcel.2004.11.032.
52. Bansbach, C.E., Bétous, R., Lovejoy, C. a., Glick, G.G., and Cortez, D. (2009). The annealing helicase SMARCAL1 maintains genome integrity at stalled replication forks. Genes Dev. *23*, 2405–2414. 10.1101/gad.1839909.
53. Mann, A., Ramirez-Otero, M.A., De Antoni, A., Hanthi, Y.W., Sannino, V., Baldi, G., Falbo, L., Schrempf, A., Bernardo, S., Loizou, J., et al. (2022). POLθ prevents MRE11-NBS1-CtIP-dependent fork breakage in the absence of BRCA2/RAD51 by filling lagging-strand gaps. Mol. Cell *82*, 4218-4231.e8. 10.1016/j.molcel.2022.09.013.
54. Schlacher, K., Christ, N., Siaud, N., Egashira, A., Wu, H., and Jasin, M. (2011). Double-Strand Break Repair-Independent Role for BRCA2 in Blocking Stalled Replication Fork Degradation by MRE11. Cell *145*, 529–542. 10.1016/j.cell.2011.03.041.
55. Tong, D., Volm, T., Eberhardt, E., Krainer, M., Leodolter, S., Kreienberg, R., and Zeillinger, R. (2003). Rad52 gene mutations in breast/ovarian cancer families and sporadic ovarian carcinoma patients. Oncol. Rep. *10*, 1551–1553.
56. Chandramouly, G., McDevitt, S., Sullivan, K., Kent, T., Luz, A., Glickman, J.F., Andrake, M., Skorski, T., and Pomerantz, R.T. (2015). Small-Molecule Disruption of RAD52 Rings as a Mechanism for Precision Medicine in BRCA-Deficient Cancers. Chem. Biol. *22*, 1491–1504. 10.1016/j.chembiol.2015.10.003.

57. Hengel, S.R., Malacaria, E., Folly da Silva Constantino, L., Bain, F.E., Diaz, A., Koch, B.G., Yu, L., Wu, M., Pichierri, P., Spies, M.A., et al. (2016). Small-molecule inhibitors identify the RAD52-ssDNA interaction as critical for recovery from replication stress and for survival of BRCA2 deficient cells. eLife *5*. 10.7554/eLife.14740.

FIGURE LEGENDS

Fig. 1 - RAD52 deficiency stimulates repriming. A. Analysis of parental ssDNA exposure by immunofluorescence. MRC5 WT were treated as indicated on the experimental scheme above. For untreated cells, Epigallocatechin (RAD52i, 50 μM) was kept for 4 hours. After the exposure to 2 mM hydroxyurea (HU), replication recovery was given by adding fresh medium. The ssDNA was detected by IdU immunofluorescence. Graph shows the intensity of ssDNA staining (AU) per cell from three replicates. Representative images are shown. Scale bar represents 10 μm. **B and C.** Analysis of parental ssDNA exposure in MRC5 shRAD52 cells. Cells were treated as indicated in A. **C.** Effect of Mirin on parental ssDNA exposure. U2OS WT were treated as indicated in A. Graph shows the intensity of ssDNA staining (AU). **D.** Analysis of parental ssDNA exposure after low dose of HU. U2OS WT were treated following the experimental scheme depicted on panel A. Graph shows the intensity of ssDNA staining (AU) per cell. Representative images are shown. Scale bar represents 10 μm. **E.** Detection of ssDNA gaps in U2OS through S1 fibers assay. On top: schemes describing the experiment. Cells were treated with or without the S1 nuclease before spreading of DNA fibers. The graph reports the mean IdU/CldU ratio. Representative images of single DNA fibers are shown. Scale bar represents 5 μm. All the values above are presented as means ± SE (ns = not significant; *P < 0.1; **P<0.1; ***P < 0.001; ****P < 0.0001; Mann–Whitney test;).

Fig. 2 – Parental DNA gaps are Polα-, but not PrimPol-, dependent in the absence of RAD52. A. Analysis of ssDNA gaps through S1 fiber assay. Wild-type MRC5 or -/- PrimPol were treated with 0.5 μM HU for 4 hours. RAD52i was given 30 min before replicative stress induction. The graph reports the mean IdU/CldU ratio. **B.** Analysis of PrimPol-ssDNA interaction using Proximity Ligation Assay (PLA). MRC5 -/- PrimPol were transfected with peGFP-PrimPol WT. 24 hours after transfection, cells were treated with 100 μM IdU for 20 hours, released for 2 hours in fresh medium and subjected to RAD52i and HU (0.5 mM). To assess PrimPol-ssDNA association, the PLA reaction was carried out using antibodies against GFP and IdU. Controls were subjected to PLA with anti-IdU or anti-GFP only. The graph reports the number of PLA spot per nucleus. Representative images are shown. **C.** Analysis of PrimPol recruitment on DNA by chromatin fractionation. MRC5 -/- PrimPol were transfected with peGFP-PrimPol WT. After 48 hours from transfection, cells were treated with RAD52i and HU (0.5 mM) for 2 and 4 hours. Cell pellets were subjected to chromatin fractionation and the protein extracts were quantified by Western Blotting. PrimPol was identified by using an antibody directed against GFP. The whole cell extracts was used as control (INPUT). **D.** Analysis of Polα-parental ssDNA interaction by PLA. U2OS WT were treated with 100 μM IdU for 20 hours, released for 2 hours in fresh medium and subjected to RAD52i and HU (0.5 mM). The PLA reaction was carried out using antibodies against the POLA1 Polα subunit and IdU. The graph reports the number of PLA spot per nucleus. The control was subjected to PLA with the anti-Polα alone. Representative images are shown. **E.** Analysis of parental ssDNA exposure in Polα-inhibited cells. U2OS WT were treated as indicated on the experimental scheme. ST1926 (Polαi) was given at 0.3 μM. Graph represents the IdU intensity (AU) per cell. Representative images are reported. **F.** Analysis of ssDNA gaps through S1 fiber assay. Wild-type MRC5 or MRC5 -/- PrimPol were treated with Polαi (0.3 μM) and RAD52i 30 min before HU (0.5 mM; 4h). The graph shows the mean IdU/CldU ratio. (ns = not significant;

*P < 0.1; **P<0.1; ***P < 0.001; ****P < 0.0001; Mann–Whitney test;). Scale bars represent 10 µm.

Fig. 3 - Polα recruitment under RAD52 deficiency depends on replication fork remodelling. A. Western blot shows the expression level of SMARCAL1 in U2OS shSMARCAL1 after 48 hours of Doxycycline (Dox, 1µg/ml) treatment. GAPDH was used as loading control. **B.** Analysis of Polα - parental ssDNA interaction by PLA in U2OS shSMARCAL1. SMARCAL1 silencing was induced by giving Doxycycline (Dox) 24 hours before treatment with IdU for 20 hours. The cells were then released for 2 hours in fresh medium and treated with or without RAD52i 30 min before giving HU (2 mM). PLA reaction was carried out using antibodies against POLA1 and IdU. Graph shows the number of PLA spot per nucleus. Representative images are shown. **C**. Analysis of Polα recruitment at DNA through chromatin fractionation. U2OS shSMARCAL1 were treated as described above. Polα was identified by using an antibody directed against the Polα subunit POLA1, and LAMIN B1 used as loading control. A graph of POLA1/LAMIN B1 quantification is reported below **D.** Analysis of Polα recruitment in ZRANB3-depleted cells by chromatin fractionation. U2OS WT were transfected with the ZRANB3 siRNA 48 hours before treatments. Polα was identified by using an antibody directed against the Polα subunit POLA1. The whole cell extracts was used as control (INPUT). **E.** Analysis of Polα-parental ssDNA in U2OS WT. Cells were treated with IdU for 20 hours, released 2 hours in fresh medium, and subjected to RAD52i and MIRIN before giving HU (2 mM). PLA reaction was carried out using antibodies against POLA1 and IdU. The graph reports the number of PLA spot per nucleus. Representative images are shown. (ns = not significant; *P < 0.1; **P<0.1; ***P < 0.001; ****P < 0.0001; Mann–Whitney test;). Scale bars represent 10 µm.

Fig. 4 - Polα-parental ssDNA association is not affected by BRC2 depletion. **A.** Western blot showing BRCA2 expression level after silencing with a siRNA. **B.** Analysis of Polα-parental ssDNA interaction in U2OS WT or transfected with BRCA2 siRNA. Transfection was carried out 24 hours before a 20 hours IdU treatment. After a release of 2 hours in fresh DMEM, cells were treated with MIRIN and HU (2 mM). PLA reaction was carried out using antibodies against POLA1 and IdU. Graph shows the number of PLA spots per nucleus. Representative images are shown. **C.** Western blot showing BRCA2 and GFP expression level. LAMIN B1 was used as loading control. **D.** Analysis of PrimPol-parental ssDNA association by PLA. MRC5 -/- PrimPol were transfected with peGFP-PrimPol WT. On the same day, cells were transfected with the BRCA2 siRNA. 24 hours after transfections, cells were treated with IdU for 20 hours, released for 2 hours in fresh medium and subjected to RAD52i or MIRIN and HU (0.5 mM). Graph shows the number of PLA spots per nucleus. **E.** Analysis of Polα-parental ssDNA interaction in MRC5 shBRCA2 and MUS81 -/-. BRCA2 silencing was obtained by treating the cells with Dox (1µg/ml) 48 hours before HU (2 mM) exposure. BRCA2 silencing was confirmed by qRT–PCR analysis of BRCA2 mRNA level 48 hours after doxycycline induction (See Fig. S7). Expression levels were normalized versus Beta-Actin gene. Relative expression levels are shown with respect to the basal level of BRCA2 in cells, which is considered as 1 (mean ±S.E.M. for n=2). PLA reaction was carried out using antibodies against POLA1 and IdU. Graph shows the number of PLA spots per nucleus. (ns = not significant; *P < 0.1; **P<0.1; ***P < 0.001; ****P < 0.0001; Mann–Whitney test;). Scale bars represent 10 µm.

Fig. 5 – RAD52 inhibition increases Polα-RAD51 association. A. Analysis of Polα-RAD51 association by PLA in U2OS WT. Cells were subjected to RAD52i 30 min before HU (2 mM) treatment. PLA reaction was carried out using antibodies against POLA1 and RAD51. The graph shows the number of PLA spot per nucleus. The control was subjected to PLA with only one primary antibody. Representative images are shown. Scale bar represents 10 µm **B.** Analysis of Polα-RAD51 association by PLA in U2OS WT. Cells were exposed to RAD52i 20 min before HU (0.5 mM) treatment of 2 and 4 hours. PLA reaction was carried out using antibodies against POLA1 and RAD51. The graph shows the number of PLA spot per nucleus. **C.** Experimental scheme of super-resolution (SR) microscopy assay. **D.** Quantification of EdU-RAD51-Polα interaction by SR microscopy (dSTORM). U2OS WT were treated as indicated on the panel C. The graph represents the percentage of variation in co-localization events of EdU-RAD51, EdU- Polα and EdU-RAD51-Polα. **E.** Representative dSTORM images of two nuclei immunolabeled for nascent DNA (cyan), Polα (magenta) and RAD51 (yellow). Scale bars = 20µm, 1µm and 100nm. A representative sketch of a common topology of the 3 signal is shown. All the values above are presented as means ± SE (ns = not significant; *P < 0.1; **P<0.1; ***P < 0.001; ****P < 0.0001; Mann–Whitney test;).

Fig. 6 - Polα engagement is mediated by RAD51. A. Analysis of Polα-parental ssDNA association by PLA. U2OS WT were treated with IdU for 20 hours, released for 2 hours in fresh DMEM and successively treated with or without RAD52i and RAD51i 30 min before HU (2 mM). The graph shows the number of PLA spot per nucleus. Representative images are shown. **B.** Analysis of Polα recruitment at the DNA by chromatin fractionation. MRC5 WT were treated with RAD52i and RAD51i 30 min before HU (2mM). Polα was identified by using an antibody directed against the Polα subunit POLA1. The whole cell extracts was used as control (INPUT). **C.** Western blot and quantification graph showing the level of RAD51 expression in RAD51 siRNA J11-transfected cells (2 pmol and 20 pmol). **D.** Analysis of Polα-parental ssDNA association by PLA in U2OS WT. Cells were transfected with the RAD51 siRNA (J11) at 2 pmol and 20 pmol 24 hours before 20 hours of IdU labelling. After 2 hours of release in fresh medium, cells were treated with RAD52i 30 min before giving HU (2 mM). PLA reaction was carried out using antibodies against POLA1 and IdU. The graph reports the number of PLA spot per nucleus. Representative images are shown. All the values above are presented as means ± SE (ns = not significant; *P < 0.1; **P<0.1; ***P < 0.001; ****P < 0.0001; Mann–Whitney or Kruskal–Wallis test;). Scale bars represent 10 µm.

Fig. 7 - Polα recruitment occurs downstream extensive replication fork degradation. A. Experimental scheme of single-cell assay for in situ Protein Interaction (SIRF). **B.** Analysis of Polα-nascent ssDNA interaction by SIRF. U2OS WT were treated as indicated above. The model on the left represents the expected background. SIRF reaction was carried out after the Click-iT™ reaction by using antibodies against POLA1 and biotin.The graph shows the mean number of SIRF spots per nucleus only of cells subjected to 5 minutes of recovery from EdU labelling. Where present, the representative images are shown above the graph. Controls were subjected to SIRF with anti-biotin only. **C.** Analysis of Polα-nascent ssDNA interaction by SIRF. U2OS WT were treated as indicated above. SIRF reaction was carried out after the Click-iT™ reaction by using antibodies against POLA1 and biotin. The graph shows the number of SIRF spots per nucleus only of cells subjected to 15 minutes of recovery from EdU labelling. Where present, the representative images are shown

above the graph. **D**. Analysis of RAD51-nascent DNA interaction by SIRF in U2OS shBRCA2. Cells were exposed to EdU labelling during all the HU treatment. SIRF reaction was carried out using antibodies against RAD51 and biotin. The graph shows the mean number of SIRF spots per cell. BRCA2 silencing was induced by giving Dox (1μg/ml) 48 hours before the experiment. BRCA2 silencing was confirmed by qRT–PCR analysis of BRCA2 mRNA level 48 hours after doxycycline induction (See sup fig 7). **E.** Analysis of RAD52-parental ssDNA interaction by PLA. U2OS WT were treated with IdU for 20 hours. After a release of 2 hours in fresh medium, cells were subjected to Polαi (ST1926, 1 μM) alone or combined with HU (0.5 or 2 mM; 2h). PLA reaction was carried out using antibodies against RAD52 and IdU. Graph shows the number of PLA spots per nucleus. Controls were subjected to PLA with anti-RAD52 only. Representative images are shown. Means ± SE are reported in scatter plots (ns = not significant; *P < 0.1; **P<0.1; ***P < 0.001; ****P < 0.0001; Mann–Whitney or Kruskal–Wallis test;). Scale bars represent 10 μm.

Fig. 8 - Polα-repriming prevents DSBs formation and chromosomal aberrations in RAD52 deficient cells. **A.** DSBs detection by immunofluorescence. U2OS WT were treated for 4h with HU and inhibitors, and recovered for 18h in drug-free medium before analysis. Immunofluorescence was carried out by using an antibody against γH2AX. The graph shows the percentage of γH2AX positive cells. Representative images are shown. **B.** Analysis of chromosomal aberrations in U2OS WT treated as in the experimental scheme above. The graphs show the mean of total chromosomal aberrations per cell and the mean of chromosomal breaks (**C**) and fusions per cell (**D**). Representative images of Giemsa-stained metaphases are given. Red arrows indicate chromosomal breaks; blue arrows indicate chromosomal fusions. Insets show an enlarged portion of the metaphases for a better evaluation of chromosomal aberrations. **E.** 53BP1 NBs detection in U2OS WT. Cells were treated as indicated in the experimental scheme above. Immunofluorescence was carried out by using an antibody against 53BP1. The graph shows the number of cells presenting 53BP1 NBs (0, 0-10 or >10). **F.** Model describing the RAD51-dependent Polα recruitment and gap formation downstream extensive degradation triggered by RAD52 deficiency. All the values above are presented as means ± SE (ns = not significant; *P < 0.1; **P<0.1; ***P < 0.001; ****P < 0.0001; Mann–Whitney or ANOVA test;). Scale bars represent 10 μm.

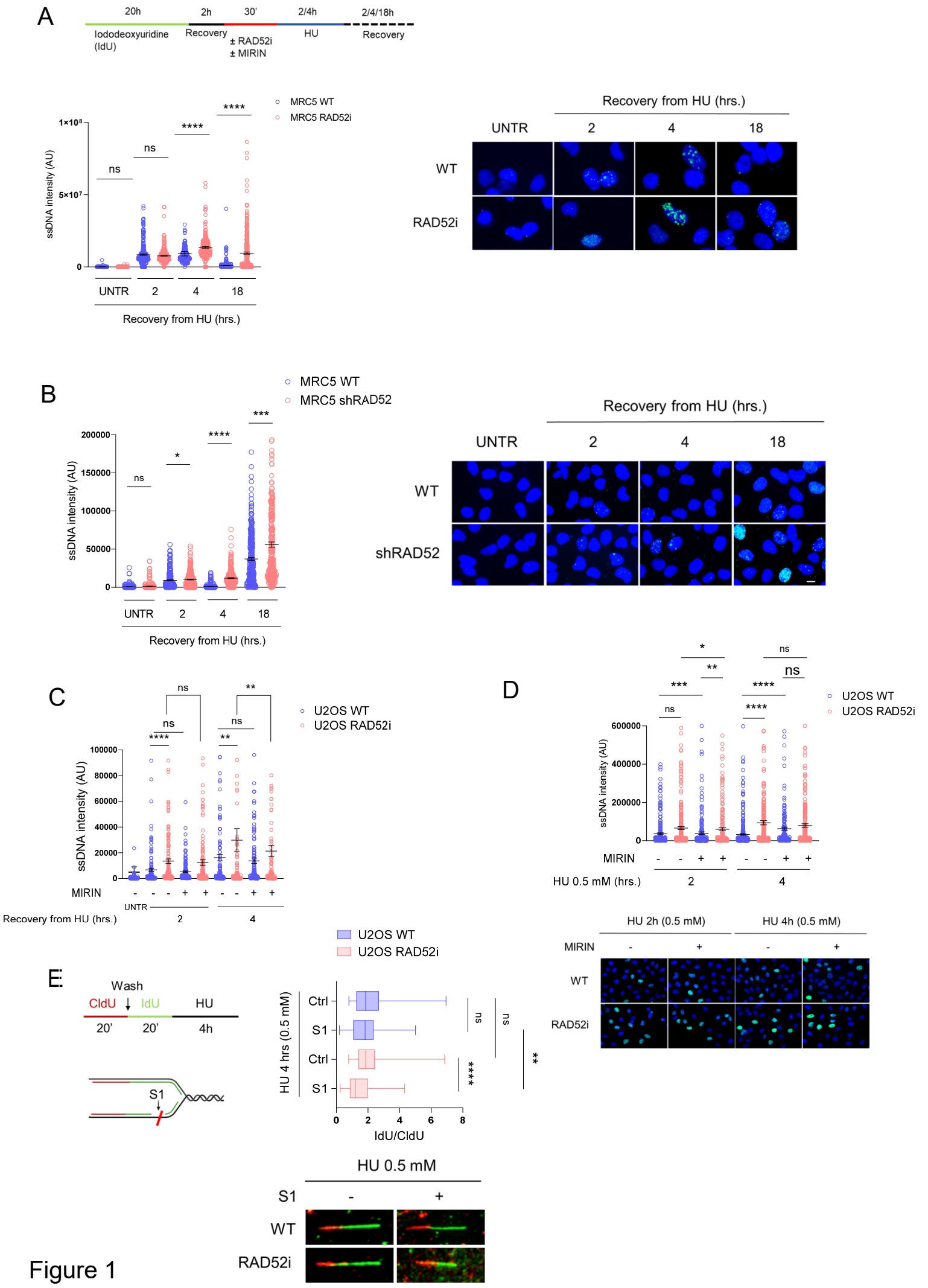
A
20h
2h
30'
2/4h
2/4/18h
Iododeoxyuridine (IdU)
Recovery
± RAD52i
± MIRIN
HU
Recovery
MRC5 WT
MRC5 RAD52i
ssDNA intensity (AU)
1×10⁸
5×10⁷
0
ns
ns
****
****
UNTR
2
4
18
Recovery from HU (hrs.)
Recovery from HU (hrs.)
UNTR
2
4
18
WT
RAD52i
B
MRC5 WT
MRC5 shRAD52
ssDNA intensity (AU)
200000
150000
100000
50000
0
ns
*
****
***
UNTR
2
4
18
Recovery from HU (hrs.)
Recovery from HU (hrs.)
UNTR
2
4
18
WT
shRAD52
C
U2OS WT
U2OS RAD52i
ssDNA intensity (AU)
100000
80000
60000
40000
20000
0
ns
ns
****
ns
**
**
MIRIN
- - - + + - - + +
UNTR
Recovery from HU (hrs.)
2
4
D
U2OS WT
U2OS RAD52i
ssDNA intensity (AU)
600000
400000
200000
0
ns
***
*
**
****
****
ns
ns
MIRIN
- - + + - - + +
HU 0.5 mM (hrs.)
2
4
HU 2h (0.5 mM)
HU 4h (0.5 mM)
MIRIN
-
+
-
+
WT
RAD52i
E
Wash
CldU
IdU
HU
20'
20'
4h
S1
U2OS WT
U2OS RAD52i
HU 4 hrs (0.5 mM)
Ctrl
S1
Ctrl
S1
ns
ns
****
**
0
2
4
6
8
IdU/CldU
HU 0.5 mM
S1
-
+
WT
RAD52i

Figure 1

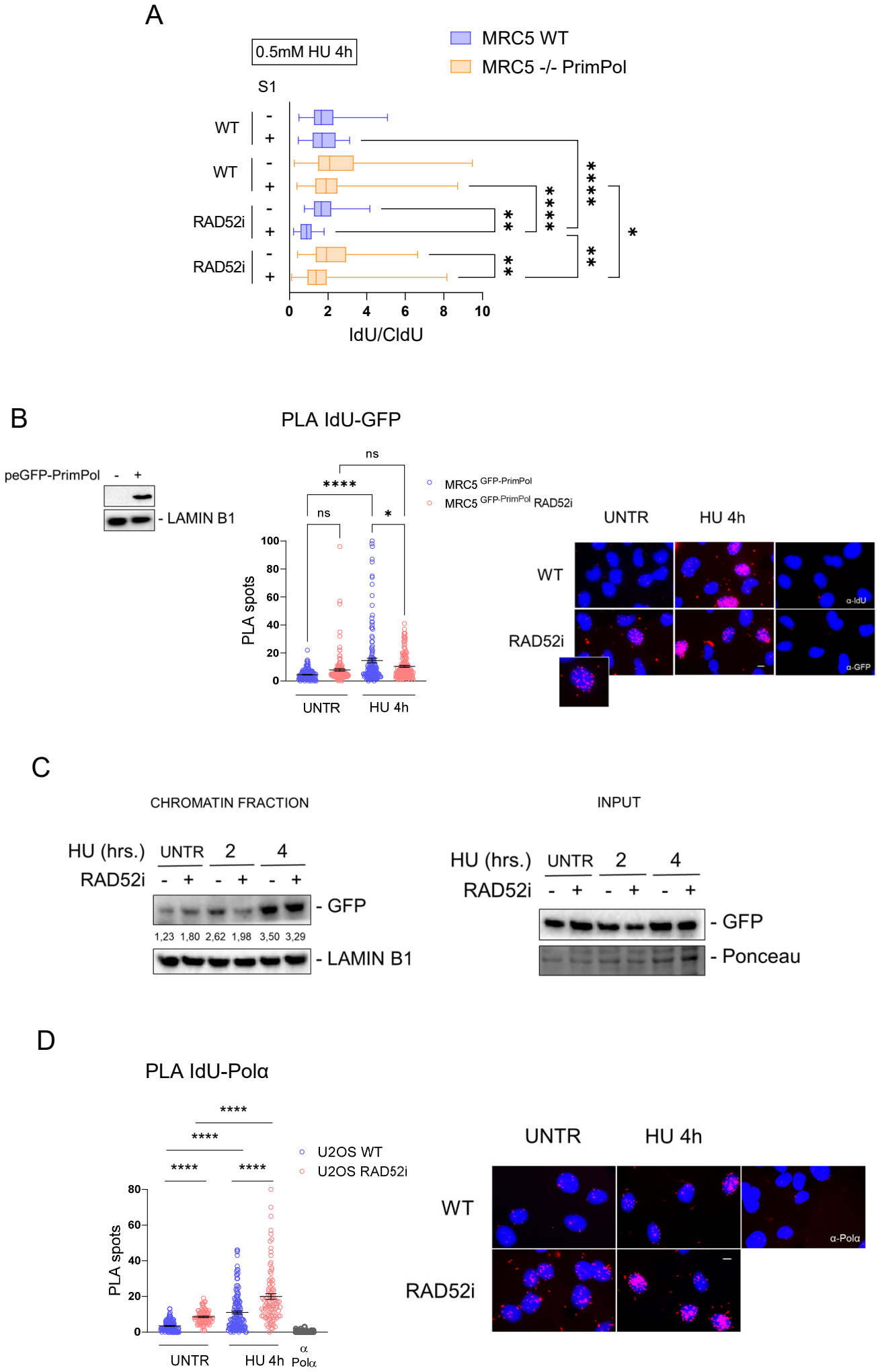
A
0.5mM HU 4h
MRC5 WT
MRC5 -/- PrimPol
S1
WT
WT
RAD52i
RAD52i
IdU/CldU
B
PLA IdU-GFP
peGFP-PrimPol
LAMIN B1
PLA spots
MRC5 GFP-PrimPol
MRC5 GFP-PrimPol RAD52i
UNTR
HU 4h
WT
RAD52i
α-IdU
α-GFP
C
CHROMATIN FRACTION
INPUT
HU (hrs.)
RAD52i
GFP
LAMIN B1
Ponceau
D
PLA IdU-Polα
U2OS WT
U2OS RAD52i
PLA spots
UNTR
HU 4h
α Polα
WT
RAD52i
α-Polα

Figure 2

E

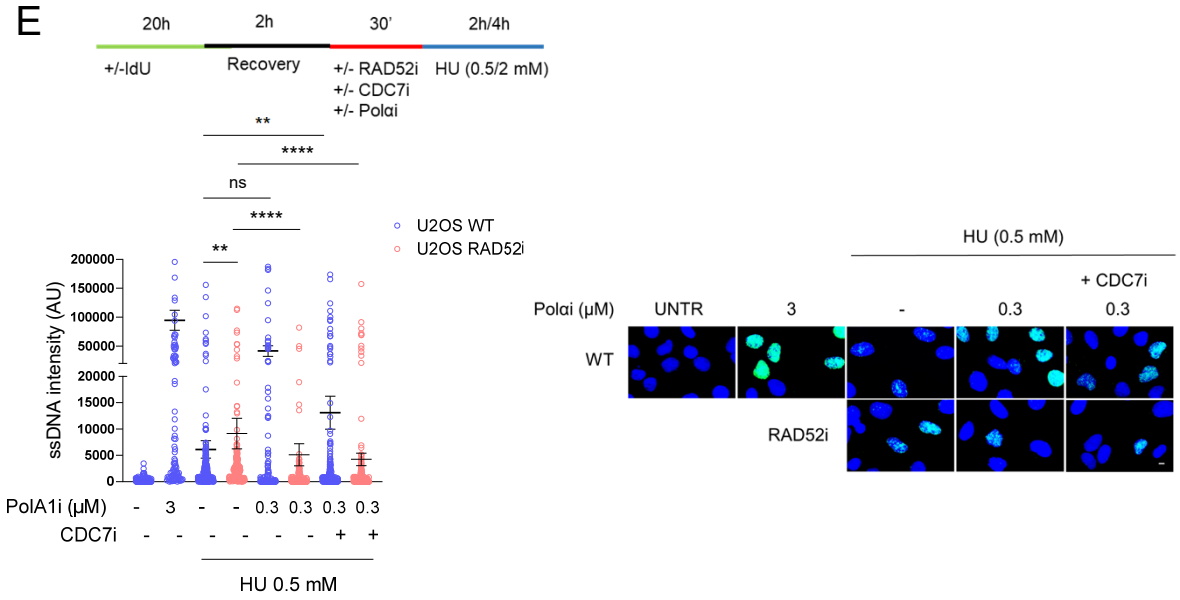

F

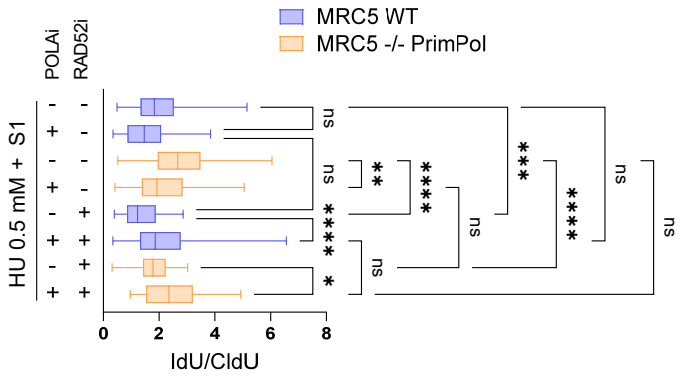

Figure 2 cont'd

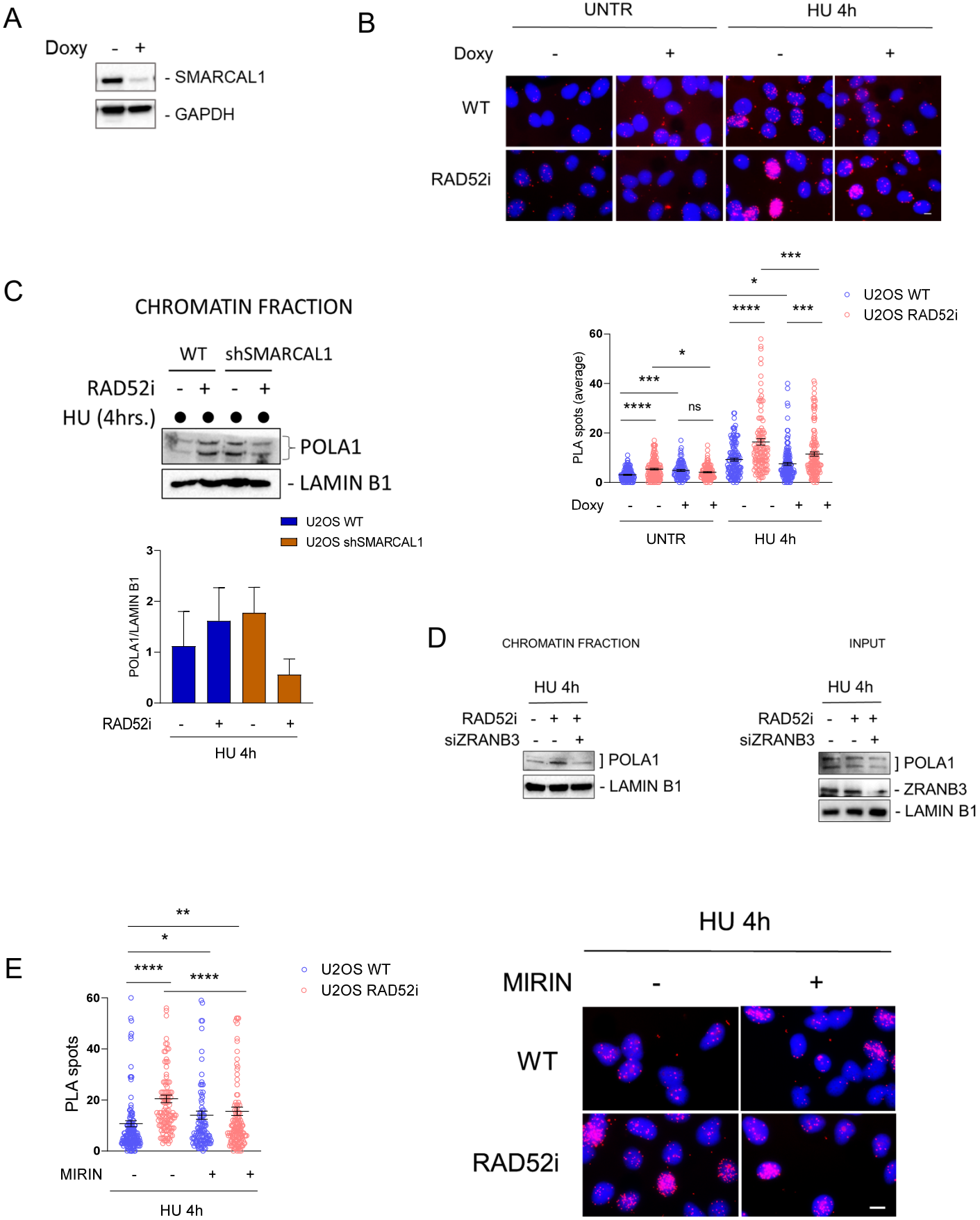
A
Doxy - +
- SMARCAL1
- GAPDH
B
UNTR
HU 4h
Doxy - + - +
WT
RAD52i
C
CHROMATIN FRACTION
WT shSMARCAL1
RAD52i - + - +
HU (4hrs.)
POLA1
- LAMIN B1
U2OS WT
U2OS shSMARCAL1
POLA1/LAMIN B1
RAD52i - + - +
HU 4h
U2OS WT
U2OS RAD52i
PLA spots (average)
Doxy - - + + - - + +
UNTR
HU 4h
D
CHROMATIN FRACTION
INPUT
HU 4h
RAD52i - + +
siZRANB3 - - +
] POLA1
- LAMIN B1
- ZRANB3
E
U2OS WT
U2OS RAD52i
PLA spots
MIRIN - - + +
HU 4h
HU 4h
MIRIN - +
WT
RAD52i

Figure 3

A

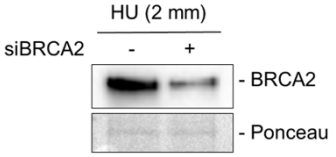

B

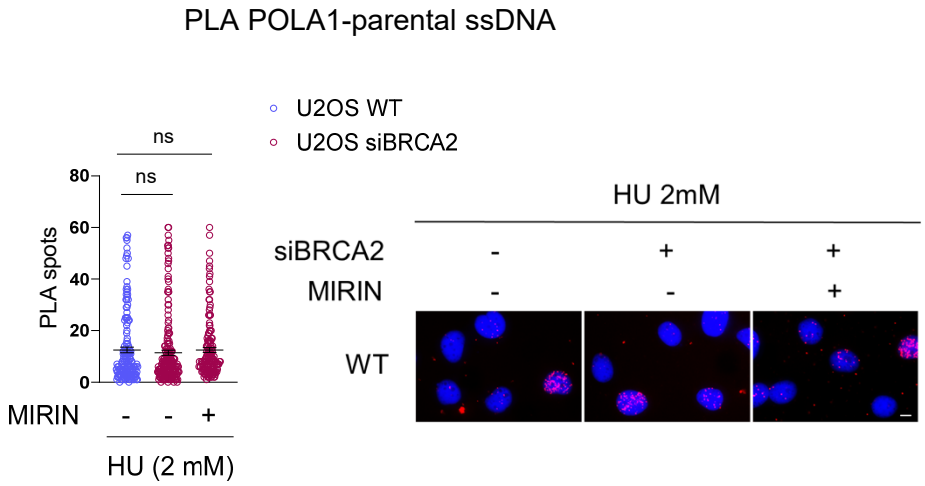

C

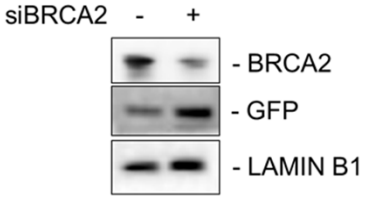

D

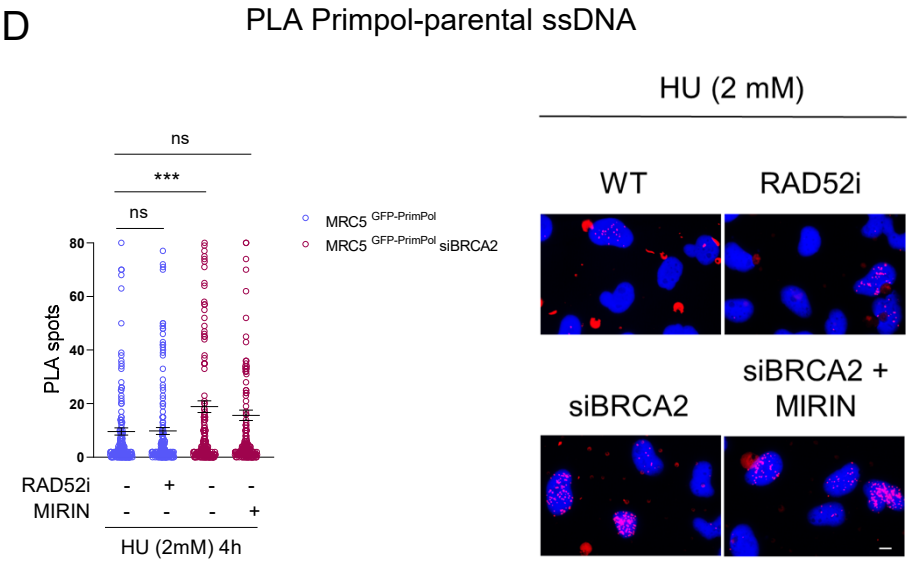

E

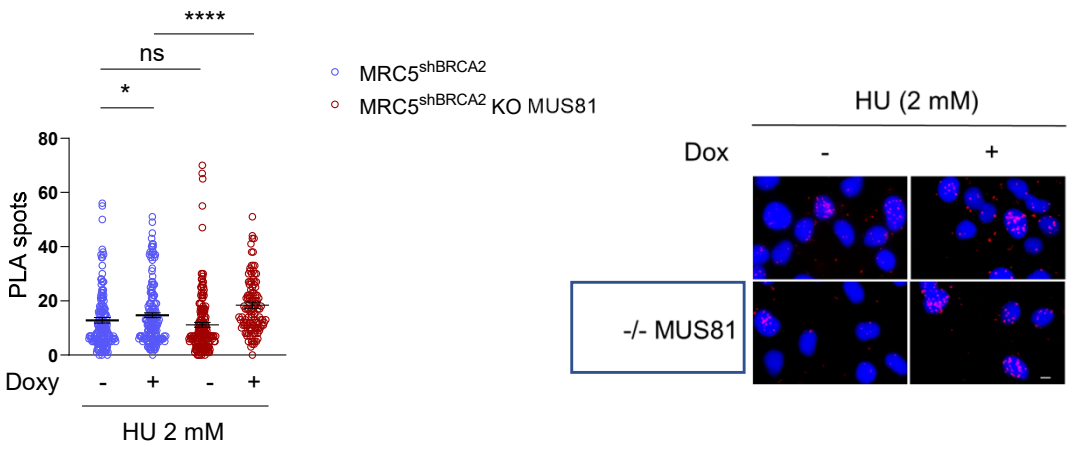

Figure 4

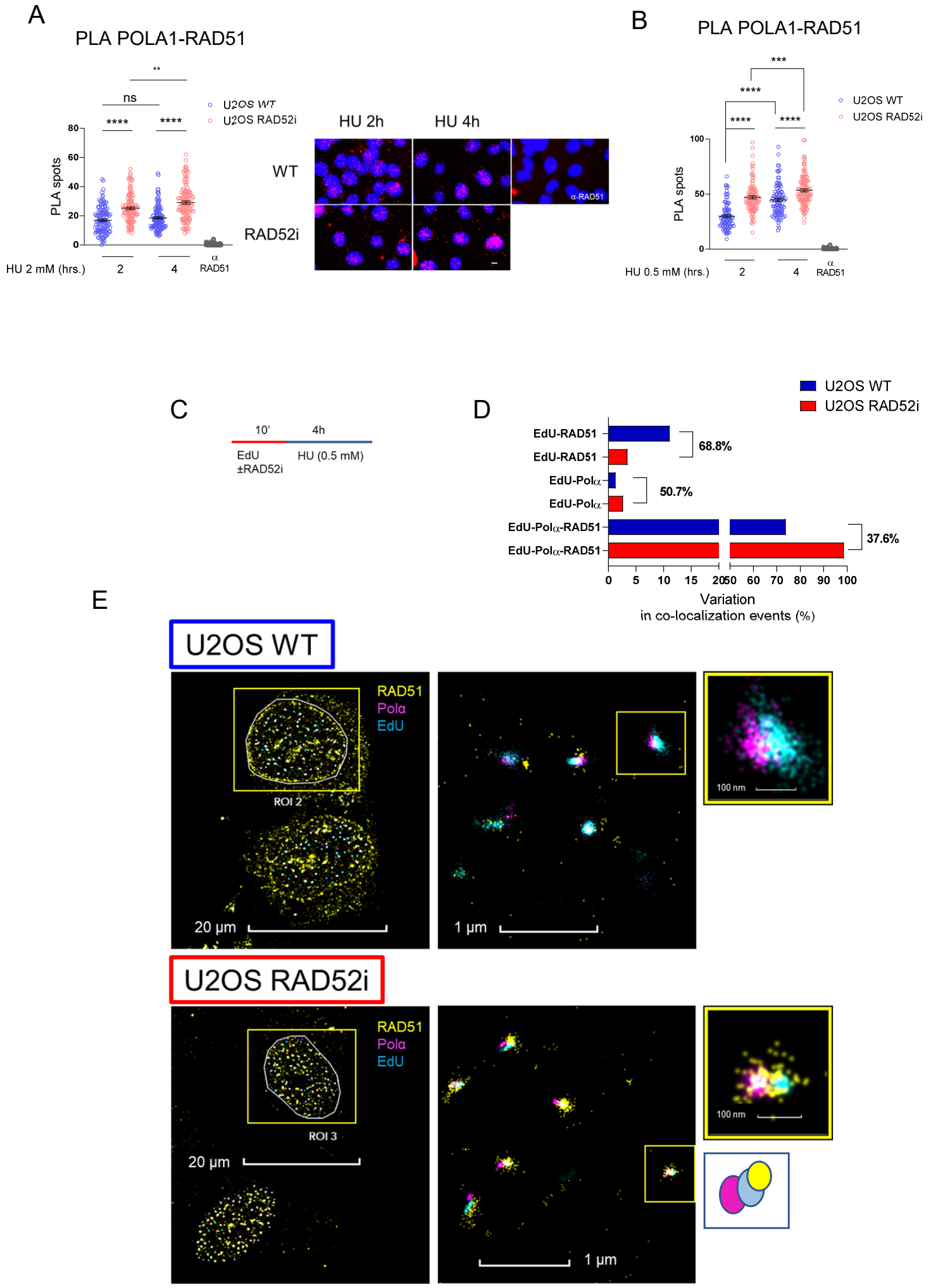
A
PLA POLA1-RAD51
U2OS WT
U2OS RAD52i
PLA spots
HU 2 mM (hrs.)
2
4
α RAD51
HU 2h
HU 4h
WT
RAD52i
α-RAD51
B
PLA POLA1-RAD51
U2OS WT
U2OS RAD52i
PLA spots
HU 0.5 mM (hrs.)
2
4
α RAD51
C
10'
4h
EdU ±RAD52i
HU (0.5 mM)
D
U2OS WT
U2OS RAD52i
EdU-RAD51
EdU-RAD51
EdU-Polα
EdU-Polα
EdU-Polα-RAD51
EdU-Polα-RAD51
68.8%
50.7%
37.6%
Variation in co-localization events (%)
E
U2OS WT
RAD51
Polα
EdU
ROI 2
20 µm
1 µm
100 nm
U2OS RAD52i
ROI 3
20 µm
1 µm
100 nm

Figure 5

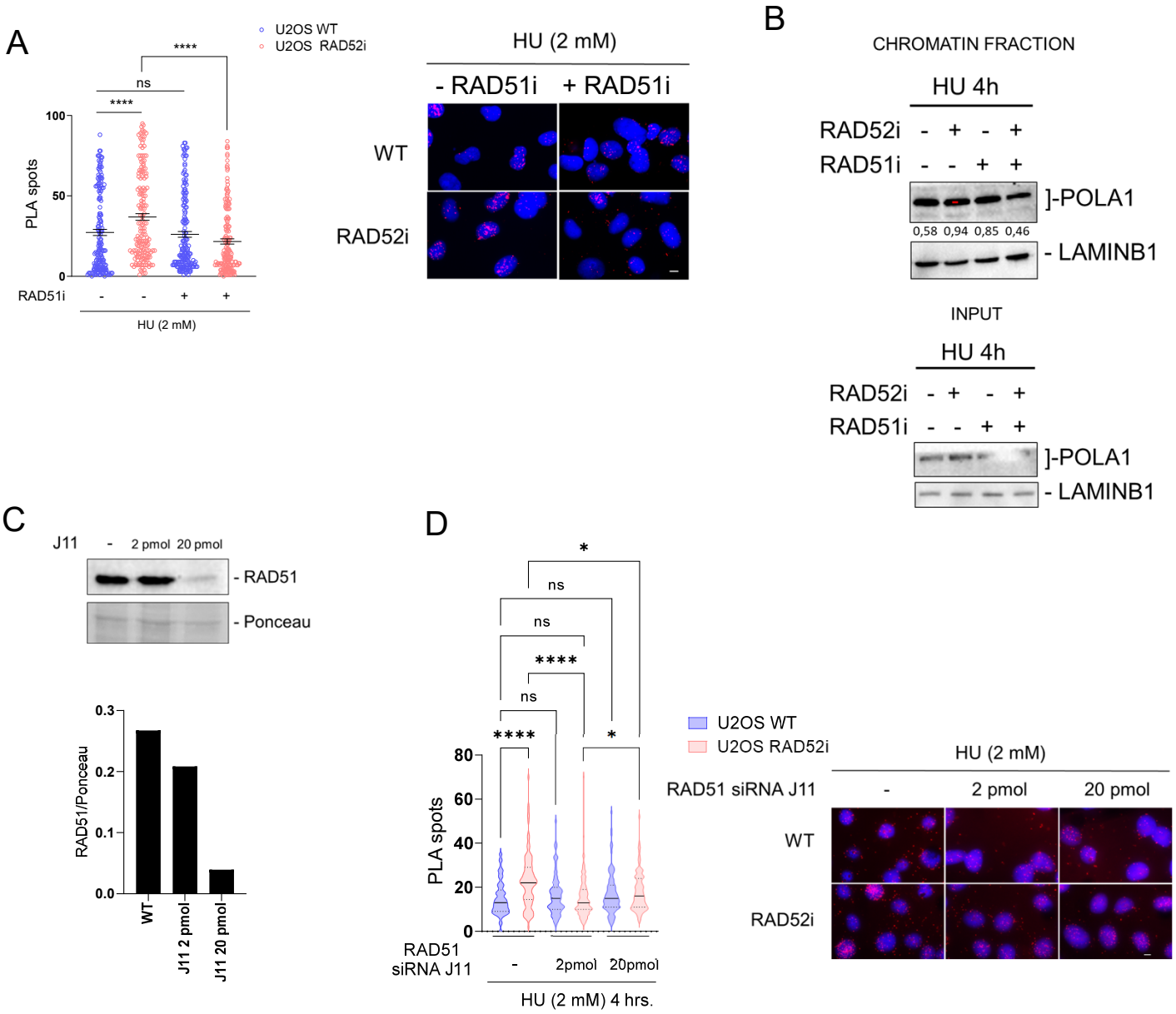
A
U2OS WT
U2OS RAD52i
PLA spots
RAD51i
HU (2 mM)
- RAD51i
+ RAD51i
WT
RAD52i
B
CHROMATIN FRACTION
HU 4h
RAD52i
RAD51i
]-POLA1
0,58 0,94 0,85 0,46
- LAMINB1
INPUT
C
J11
2 pmol
20 pmol
- RAD51
- Ponceau
RAD51/Ponceau
D
U2OS WT
U2OS RAD52i
RAD51 siRNA J11
HU (2 mM) 4 hrs.

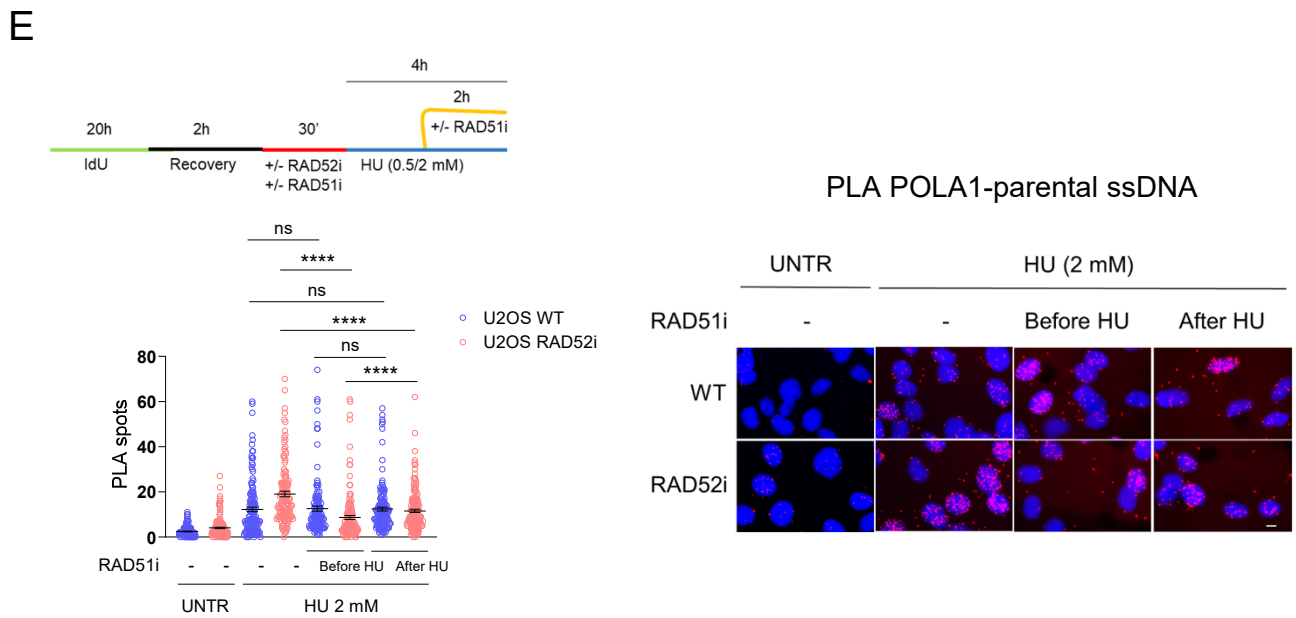
E
4h
2h
20h
30'
+/- RAD51i
IdU
Recovery
+/- RAD52i
+/- RAD51i
HU (0.5/2 mM)
PLA POLA1-parental ssDNA
UNTR
HU (2 mM)
Before HU
After HU
HU 2 mM

Figure 6

A

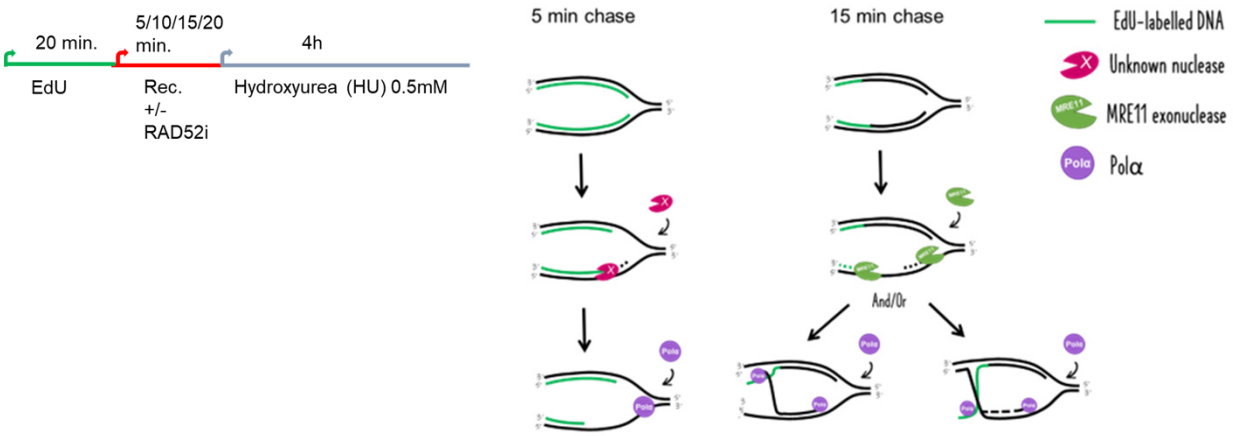

B

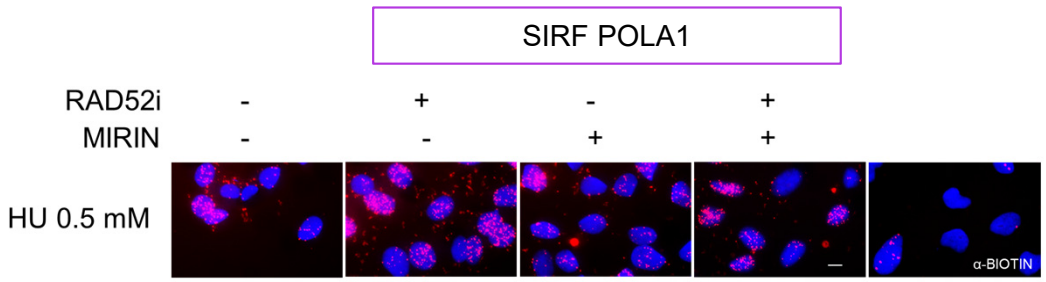

5 min chase

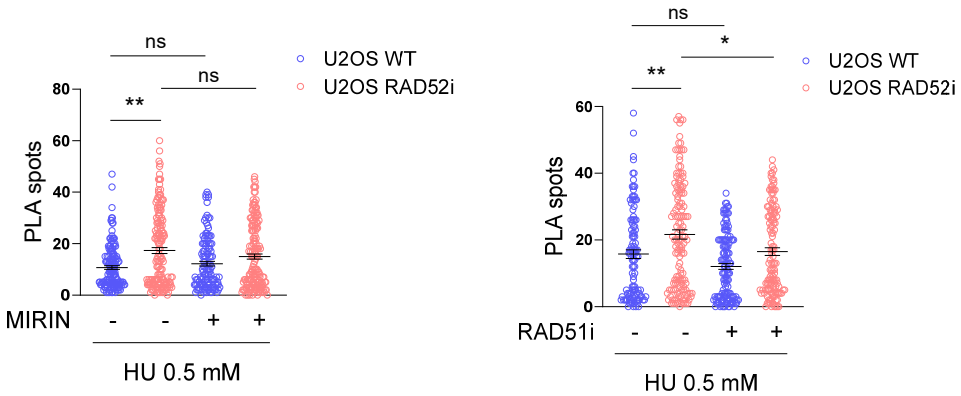

C

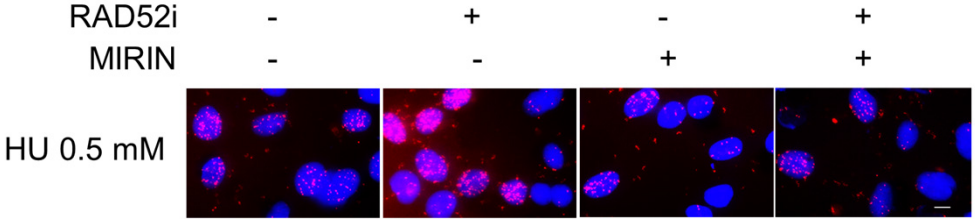

15 min chase

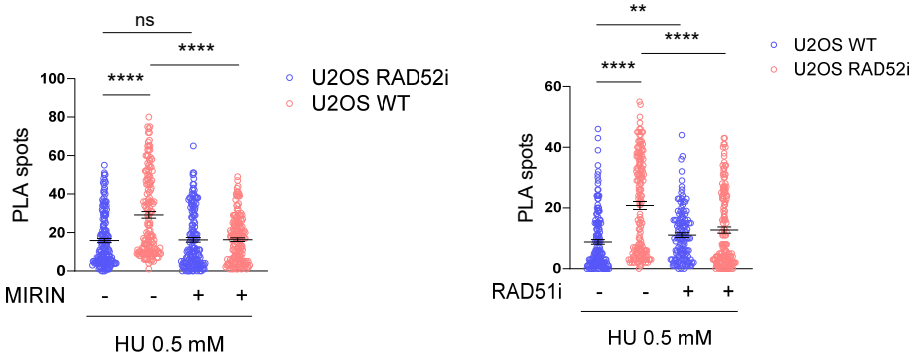

Figure 7

D

SIRF RAD51

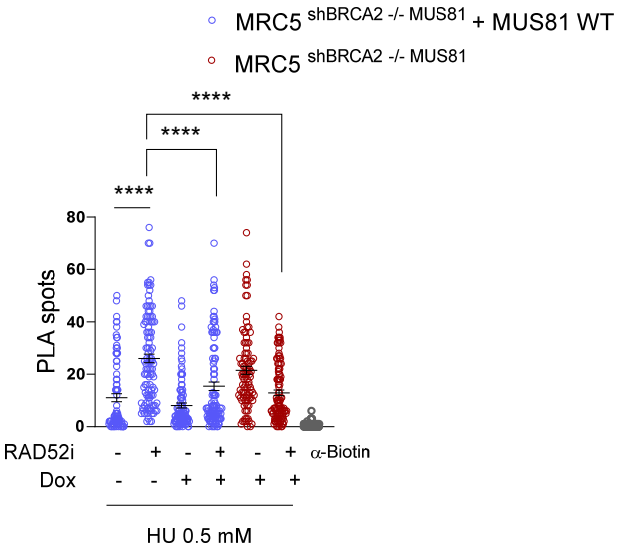

E

PLA RAD52-parental ssDNA

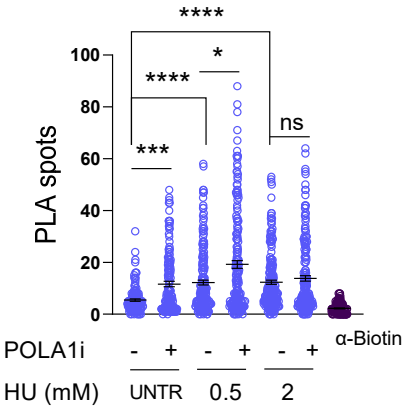

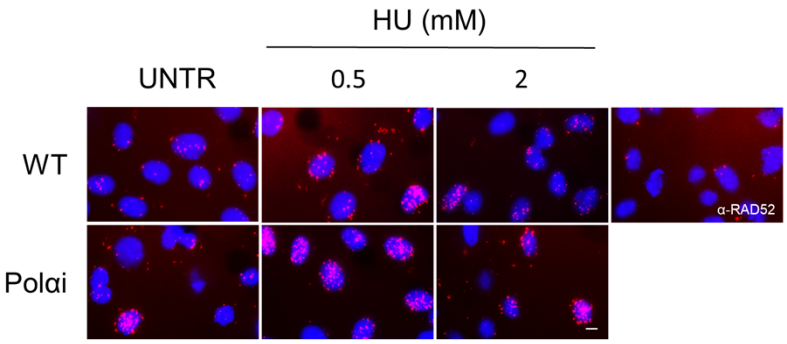

Figure 7 cont'd

A

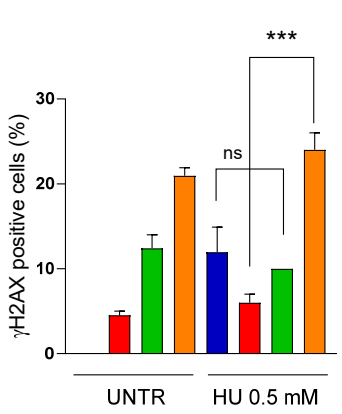

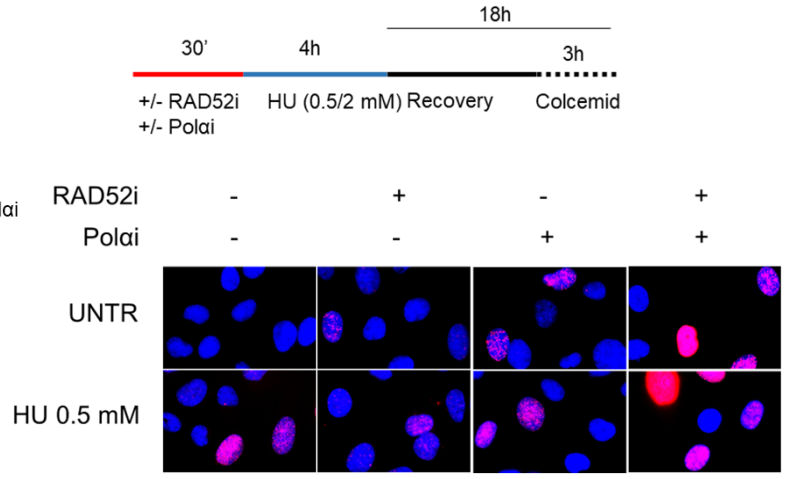

B

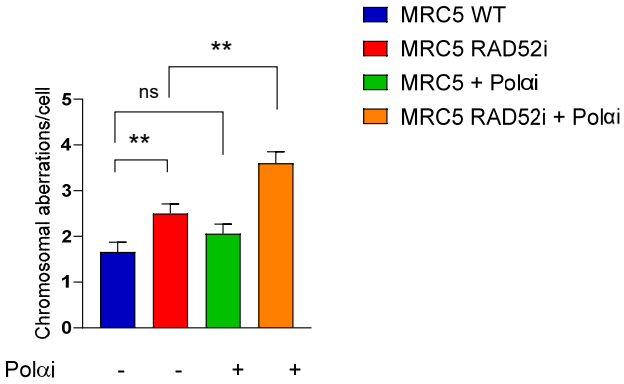

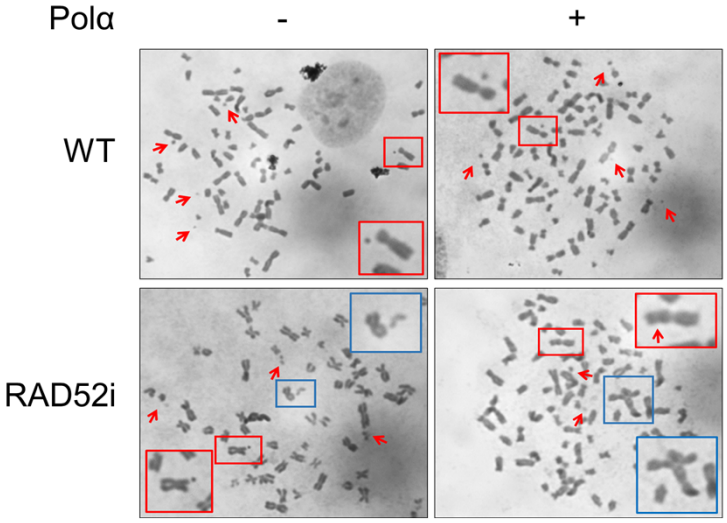

C

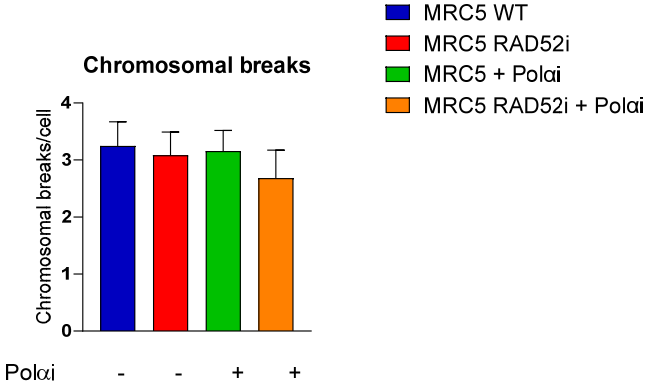

D

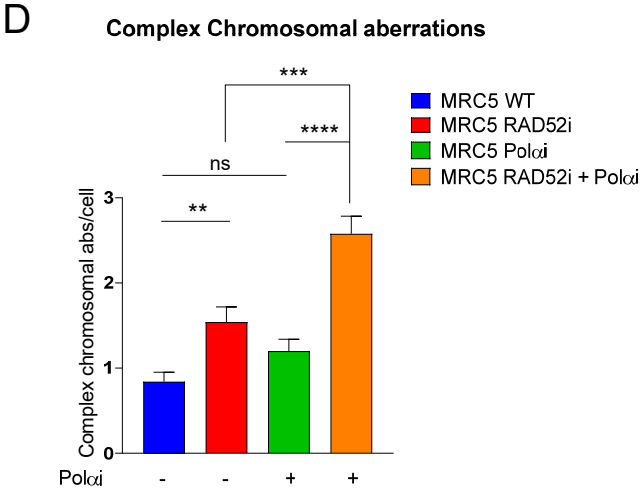

E

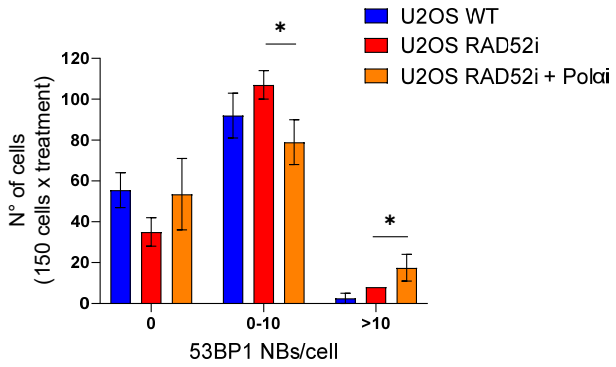

Figure 8

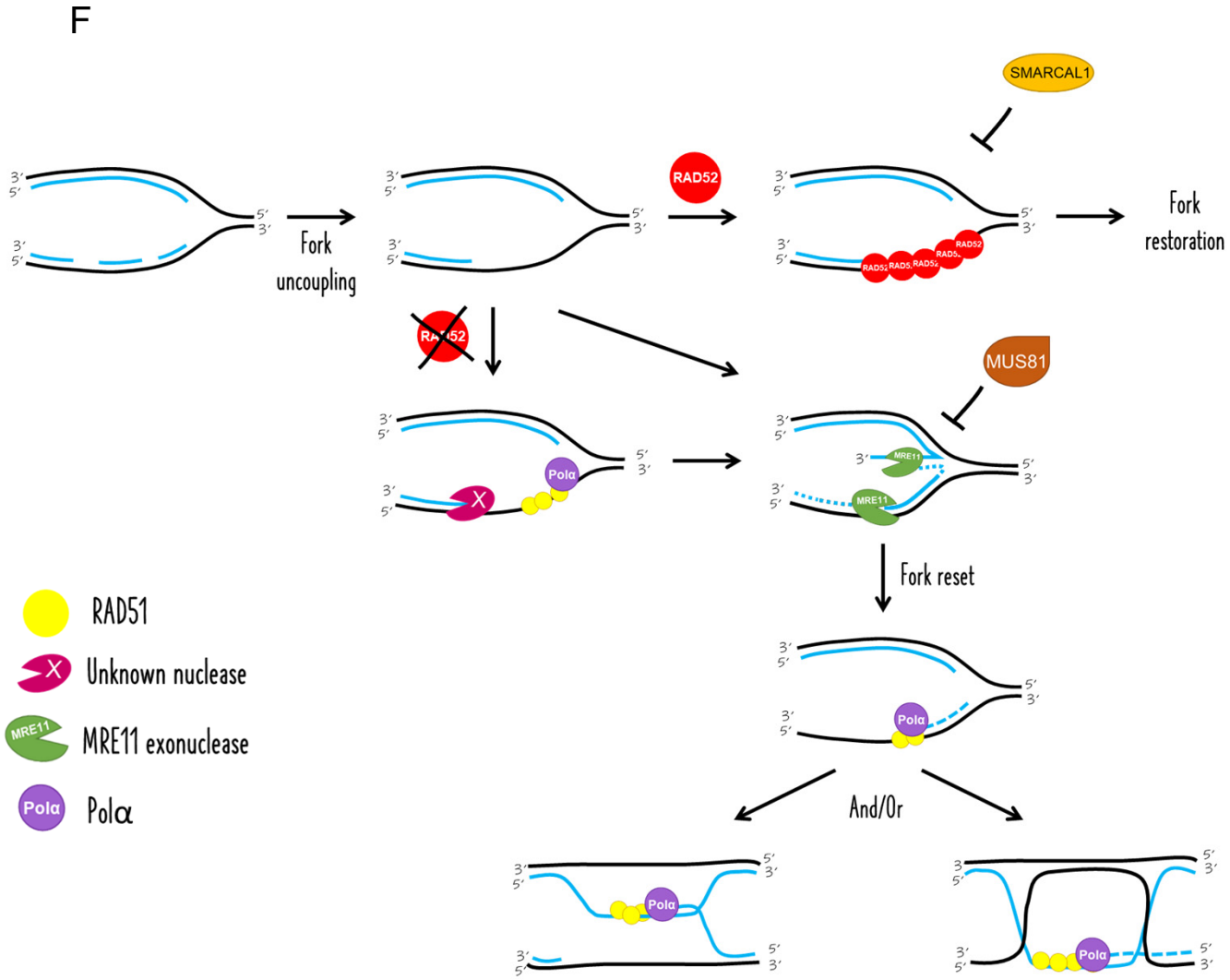
F
SMARCAL1
RAD52
Fork uncoupling
Fork restoration
MUS81
Polα
MRE11
Fork reset
And/Or
RAD51
Unknown nuclease
MRE11 exonuclease
Polα

Figure 8